

# Deciphering the Origin of the Regular Satellites of Gaseous Giants – Iapetus: the Rosetta Ice-Moon

Ignacio Mosqueira and Paul R. Estrada  
Carl Sagan Center, SETI Institute

and

Sebastien Charnoz  
Université Paris Diderot/CEA/CNRS

August 2009

## Abstract

Ever since their discovery the regular satellites of Jupiter and Saturn have held out the promise of providing an independent set of observations with which to test theories of planet formation. Yet elucidating their origin has proven elusive. Here we show that Iapetus can serve to discriminate between satellite formation models. Its accretion history can be understood in terms of a two-component gaseous subnebula, with a relatively dense inner region, and an extended tail out to the location of the irregular satellites, as in the SEMM model of Mosqueira and Estrada (2003a,b). Following giant planet formation, planetesimals in the feeding zone of Jupiter and Saturn become dynamically excited, and undergo a collisional cascade. Ablation and capture of planetesimal fragments crossing the gaseous circumplanetary disks delivers enough collisional rubble to account for the mass budgets of the regular satellites of Jupiter and Saturn. This process can result in rock/ice fractionation as long as the make up of the population of disk crossers is non-homogeneous, thus offering a natural explanation for the marked compositional differences between outer solar nebula objects and those that accreted in the subnebulae of the giant planets. For a given size, icy objects are easier to capture and to ablate, likely resulting in an overall enrichment of ice in the subnebula. Furthermore, capture and ablation of rocky fragments become inefficient far from the planet for two reasons: the gas surface density of the subnebula is taken to drop outside the centrifugal radius, and the velocity of interlopers decreases with distance from the planet. Thus, rocky objects crossing the outer disks of Jupiter and Saturn never reach a temperature high enough to ablate either due to melting or vaporization, and capture is also greatly diminished there. In contrast, icy objects crossing the outer disks of each planet ablate due to the melting and vaporization of water-ice. Consequently, our model leads to an enhancement of the ice content of Iapetus, and to a lesser degree those of Titan, Callisto and Ganymede, and accounts for the (non-stochastic) compositions of these large, low-porosity outer regular satellites of Jupiter and Saturn. For this to work, the primordial population of planetesimals in the Jupiter-Saturn region must be *partially* differentiated, so that the ensuing collisional cascade produces an icy population of  $\gtrsim 1$  m size fragments to be ablated

during subnebula crossing. We argue this is likely because the first generation of solar nebula  $\sim 10$  km planetesimals in the Jupiter-Saturn region incorporated significant quantities of  $^{26}\text{Al}$ . This is the first study successfully to provide a direct connection between nebula planetesimals and subnebulae mixtures with quantifiable and observable consequences for the bulk properties of the regular satellites of Jupiter and Saturn, and the *only* explanation presently available for Iapetus' low density and ice-rich composition.

# 1 Formation of the Regular Satellites of Giant Planets

The regular satellites orbit in the prograde direction, meaning the same sense of rotation as the spin of the primary, and lie close to the Laplace surface, with the exception of Saturn’s Iapetus (whose orbit is nearly circular with an eccentricity of  $e = 0.028$  but inclined  $i = 7.5^\circ$  with respect to the Laplace surface). Broadly speaking, the interpretation of these observations is straightforward: unlike the irregular satellites, which tend to have inclined and distant orbits and represent a population of captured objects, the regular satellites form in circumplanetary disks of gas and solids. Notably, the regular satellite systems of Jupiter and Saturn share a number of similarities, including the mass ratio of the largest satellites to the primary, the specific angular momentum, and bulk compositions. Yet, the differences are also striking: a trend of decreasing density with radial distance is apparent for the Jovian but not the Kronian regular satellites; and the mass ratio between Ganymede and the other Galilean satellites is not nearly as extreme as that between Titan and its neighbors. Indeed, Titan’s isolation, the compositional diversity of Saturn’s inner moons as well as its ring system may attest to titanic clashes between the well-behaved residents proper and unruly foreign hordes – interlopers from the outer solar system wreaking-havoc upon the planet’s orderly retinue. In its remote outpost, Iapetus, a survivor of the onslaught, icily bears witness to that early violent epoch, as its battle-scarred surface records. Iapetus’ extreme albedo contrast, large separation from Saturn and other Saturnian moons, its low eccentricity yet significant inclination, its frozen-in shape and equatorial ridge, its ancient, cratered surface, and icy composition all combine to make it a Rosetta moon. It is to this mysterious, two-faced sentinel of the outer solar system that we primarily turn our attention.

Observational evidence indicates that the largest KBOs are of different composition than the regular satellites of the giant planets. Triton ( $\rho = 2.061 \pm 0.007 \text{ g cm}^{-3}$ ; Person et al. 2006), Eris ( $\rho = 2.3 \pm 0.3 \text{ g cm}^{-3}$ ; Brown and Schaller 2007), and Pluto-Charon ( $\rho = 1.94 \pm 0.09 \text{ g cm}^{-3}$ ; Buie et al. 2006) have densities that imply a rock/water-ice ratio of approximately 70/30 by mass. These high densities have long been interpreted to result from accretion in the outer solar system given the presence of abundant, oxygen-sequestering uncondensed CO (Prinn and Fegley 1981; McKinnon et al. 1997). In contrast, Ganymede ( $\rho = 1.94 \text{ g cm}^{-3}$ ) and Callisto ( $\rho = 1.83 \text{ g cm}^{-3}$ ) each consist of  $\sim 50/50$  rock/water-ice by mass, with Ganymede being slightly more rock-rich (Sohl et al. 2002). Similarly, Titan ( $\rho = 1.88 \text{ g cm}^{-3}$ ) is also half-rock/half-ice by mass. The simplest explanation of these observations is that the subnebulae of the giant planet were enriched in water-ice compared to the outer solar nebula, although this interpretation is partly clouded by uncertainties in our present understanding of solar abundances (e.g., Wong et al. 2008).

Further insight can be sought from other regular satellites. The inner satellites of Jupiter, Io and Europa, may have lost volatiles either due to the temperature gradient in the subnebula (Pollack et al. 1976; Lunine and Stevenson 1982), collisional processes involving differentiated objects, and/or the Laplace resonance<sup>1</sup>. Switching over to Saturn, the observed densities of the medium-sized regular satellites are not compatible with solar composition (Wong et al. 2008). It has long been argued that these observations are consistent with

---

<sup>1</sup>Amalthea may have incorporated water-ice (Anderson et al. 2005), but it is unclear how much. Amalthea may be too small and close to the planet to provide a useful constraint on satellite formation theories.

accretion in a reducing subnebula with efficient conversion of CO to CH<sub>4</sub> (as opposed to inhibited conversion in the solar nebula; Prinn and Fegley 1981). However, satellite formation models do not provide an environment that can support such chemistry (Estrada et al. 2009). Also, close-in to Saturn collisional processes and/or resonances (at least in the case of Enceladus) appear to have resulted in a stochastic component<sup>2</sup>.

Yet, Iapetus would not be affected by these processes, and it is large enough to provide a sample of the composition of the outer disk of Saturn. Iapetus is different from other regular satellites largely by virtue of its distance from the planet: it may have survived the early bombardment because impact speeds at its location are significantly slower than those closer in to Saturn, where the gravitational well leads to hypervelocity impacts; its frozen-in shape and unique ridge are likely associated with its location far from Saturn (Castillo-Rogez et al. 2007); its significant inclination is likely connected with the deviation of the Laplace plane away from the planet’s equator plane at its location (Ward 1981 but note that this scenario requires a subnebula dispersal time of  $\lesssim 10^3$  yr; Tremaine et al. 2009); its large albedo contrast is likely ultimately due to the deposition of exogenous material on the surface of this tidally-locked regular satellite (Burns et al. 2009; Buratti et al. 2009); and, as we show here, its composition too is tied to its location in the Kronian subnebula. These properties taken together with the difficulty inherent in the capture of a such a large body into a low-eccentricity orbit provide a compelling case for *in situ* accretion in a circumplanetary disk of gas and dust<sup>3</sup>.

To establish a connection to the outer Kronian subnebula we must first constrain Iapetus’ porosity. Given its mean radius and mean density ( $r = 736.0 \pm 2$  km and  $\rho = 1.081 \pm 18$  g cm<sup>-3</sup>; Thomas et al. 2006) the pressure at the core ( $P = (2\pi/3)\rho^2 Gr^2 \simeq 100$  MPa) is high enough that porosity should be small there (though it could be larger in the outer layers of the satellite). Experimental results indicate a reduction in porosity in cold, granular water ice over a pressure range of  $\sim 1 - 150$  MPa, with porosities of the order of  $\sim 10\%$  for  $\sim 100$  MPa pressures (Durham et al. 2005). Heating, annealing and creep-driven water-ice flow can result in pore collapse and decrease the porosity even more. Models in which Iapetus de-spins due to the presence of short-lived radioactive isotopes (SLRI), leading to the formation of a ridge, imply warm-ice and low porosities (Castillo-Rogez et al. 2007; Melosh and Nimmo 2009). Although the rheology of icy satellites is poorly understood, the interpretation of Iapetus’ fossil shape as “frozen-in” due to lithospheric hardening as the satellite was in the process of despinning is persuasive, and at odds with with a high-porosity object. Note that weak radiogenic heating due to long-lived radioactive isotopes (LLRI) alone would be enough to collapse the pores except in a surface layer tens of kilometers thick (Castillo-Rogez et al. 2007). An Iapetus’ model with a porosity of  $\sim 0.3$  in a clean-ice upper  $\sim 50$  km (roughly the surface layer thickness of the Castillo-Rogez et al. (2007) LLRI model; cf their Fig. 6) of the satellite would result in a rock ratio of  $\sim 30\%$  by mass, which is still rock-depleted compared to Ganymede, Titan and Callisto. Furthermore, even if it were possible to despin a cold Iapetus, the presence of the ridge is likely to indicate ice mobility early on. Thus, we

---

<sup>2</sup>See Mosqueira and Estrada 2003b for an alternative explanation for the ice-rich composition of close-in, mid-size Saturnian regular satellites.

<sup>3</sup>Elsewhere (Mosqueira and Estrada 2005), we discuss an intriguing collisional-scattering scenario for the origin of Iapetus; however, we favor the present model.

argue that Iapetus is an icy satellite with rock/water-ice fraction of  $\sim 20\%$  by mass, making its composition incompatible with solar mixtures (Wong et al. 2008).

We stress that Iapetus' low density relative to Titan, Ganymede and Callisto *cannot* be explained by a snowline argument since all four satellites are taken to accrete outside the snowline (Pollack 1976; Lunine and Stevenson 1982). The issue here is the depletion of rock, as opposed to the presence of volatiles, in Iapetus. In this regard, it is instructive to compare Iapetus to irregular Phoebe. The Cassini flyby of Phoebe yielded a density of  $1.630 \pm 0.046 \text{ g cm}^{-3}$  (Jacobson et al. 2006). If we allow for a moderate porosity, which is reasonable given its  $106.60 \pm 1.00 \text{ km}$  size, this density corresponds to a rock/water-ice fraction similar to that of large KBOs. The contrast between Iapetus and Phoebe reinforces the interpretation of Phoebe as a captured moon from the outer solar nebula (Johnson and Lunine 2005). Indeed, the rock/water-ice fraction for Phoebe may be larger than those of Ganymede, Callisto and Titan. Allowing for significant porosity in the case of Phoebe would accentuate the compositional contrast with Iapetus and other regular satellites.

In the nucleated instability model of planet formation (e.g., Bodenheimer and Pollack 1986; Pollack et al. 1996) a core must first form by accretion of planetesimals. In this mode of planet formation most of the mass of solids resides in planetesimals of size  $\sim 10 \text{ km}$  (Wetherill and Stewart 1993). Planetesimals are also needed to explain the observations of the Oort cloud and the scattered belt (e.g., Charnoz and Morbidelli 2007), to power planet migration in the Nice model (e.g., Morbidelli et al. 2008), and to explain the volatile enhancement in giant planet atmospheres by planetesimal trapping and delivery (e.g., Owen and Encrenaz 2003). Here we seek to provide a direct physical link between planetesimals in the solar nebula and the circumplanetary disks of giant planets, and to account for the source of the solids that ultimately led to the formation of the regular satellites of the giant planets. Our aim is to study mass delivery by ablation of planetesimal fragments crossing the circumplanetary disk (to be followed by re-condensation and satellite accretion). In particular, ablation can result in fractionation, and account for the observed density of Iapetus provided that this satellite formed *in situ* (Mosqueira and Estrada, 2005). Although we focus on Iapetus, our model applies to the origin of the regular satellites in general<sup>4</sup>. The model we present here fits with the gaseous SEMM satellite formation model (Mosqueira and Estrada 2003a,b; hereafter MEa,b; see also Estrada et al. 2009 and Mosqueira et al. 2009). This framework is consistent with the core accretion planet formation model in which Jupiter and Saturn form  $\sim 3 - 5 \text{ Myr}$  after CAIs (Hubickyj et al. 2005; Dodson-Robinson et al. 2008). Note that in alternative *gas-poor* or *gas-starved* satellite formation models planetesimals do not traverse enough subnebula gas to ablate significantly. Thus, mass delivery by ablation is not available to these models whether they consider planetesimals as a source of solids (Estrada and Mosqueira 2006) or not (Canup and Ward 2002).

For rock/water-ice fractionation to take place, and our Iapetus' model to obtain, the first generation of planetesimals in the Jupiter-Saturn region must incorporate significant

---

<sup>4</sup>For instance, the puzzling observation that primordial  $^{36}\text{Ar}$  is enhanced in the atmosphere of Jupiter (Atreya et al. 1999), but only present in trace amounts in the atmosphere of Titan, as reported by the GCMS instrument aboard Cassini (Niemann et al. 2005), may fit within a framework of planetesimal ablation followed by subnebula re-condensation of some volatiles but not others, but we leave this subject for further work.

quantities of  $^{26}\text{Al}$ , which depends on their time of formation. The closest analog to the planetesimals forming in the Jupiter-Saturn region is the asteroid belt. The ages of asteroids indicate that they formed with a spread of 1 – 3 Myr after Ca-Al-rich inclusions (CAIs) (Scott and Krot 2005). The asteroid belt may have been cleared largely by scattering due to planetary embryos and a migrating Jupiter (Bottke et al. 2005). Yet, the fossil evidence provided by asteroids may not be directly linked to the first generation of planetesimals. (It is worth noting that the parent bodies of iron meteorites may have formed 1 – 2 Myr earlier than those of the ordinary chondrites; Baker et al. 2005.) Instead, main belt asteroids are the product of a few My of accretion before most of the mass in the belt was depleted (Weidenschilling 2009). Indeed, as runaway growth proceeds to completion most small bodies would be ground down by embryos. The degree of collisional evolution in asteroidal objects depends on the size of the planetesimals, which may be used to provide a constraint of  $\sim 10 - 100$  km on primordial planetesimal sizes (Weidenschilling 2009). Thus, neither asteroids nor meteorites provide a direct sample of this population. Nevertheless, iron meteorites may have come from  $\sim 20 - 200$  km differentiated parent bodies that underwent catastrophic collisions (Chabot and Haack 2006).

The timescale for the formation of planetesimals depends on the nebular environment early on. Assuming efficient sticking, the timescale for the formation of planetesimals is very short indeed  $\tau \sim 2000 (a/1 \text{ AU})^{3/2}$  years, where  $a$  is the radial distance from the Sun (Weidenschilling 2000). Collisional growth appears to be efficient for small particle sizes and impact speeds (see review by Dominik et al. 2007); yet, growth past the decoupling size  $\sim 1$  m in the presence of turbulence is questionable (Mosqueira 2004; Cuzzi and Weidenschilling 2006). The problem is especially severe in light of the short clearing times of  $\sim 1$  m size objects. It can be argued that in the presence of turbulence planetesimals can bypass this size range entirely (Johansen et al. 2007; Cuzzi et al. 2008), however there is no agreement regarding the specific mechanism to accomplish this leap – the simulations of Johansen et al. (2007) *assume* a particle size that is already partially decoupled from the gas, whereas the simulations of Cuzzi et al. (2008) do not yet show that a large planetesimal  $\gtrsim 10$  km can actually form (even sporadically) from chondrule-like  $\sim 1$  mm sized particles. While a recent study concludes that asteroids are born big (Morbidelli et al. 2009), given uncertainties in the strength of planetesimals and the role of collisional debris, the asteroid size distribution, and the timing of the excitation caused by the migration of Jupiter, planetesimal sizes 10 – 100 km appear consistent with the data. In this regard, the possibility should be explored that smaller planetesimals are disrupted by planetary embryos prior to the final stages of asteroid accretion.

The alternative that quiescent regions can help to form planetesimals has been considered in a number of publications (Kretke and Lin 2007; Brauer et al. 2008; Lyra et al. 2009). The stumbling block here may be an embarrassment of riches, i.e., in a laminar disk it is *too easy* to make planetesimals. Consequently, dust might coagulate into larger objects too fast to explain the observations of protoplanetary disks indicating the presence of small  $\lesssim 3 \mu\text{m}$  grains (e.g., Dullemond and Dominik 2005; Cuzzi et al. 2008; Birnstiel et al. 2009), the evidence for *delayed* ( $\sim 1$  Myr) grain growth based on observations of SEDs of young disks (Beckwith et al. 2000; Currie et al. 2009), or the lack of pervasive differentiation of main belt asteroids (Cuzzi et al. 2008). However, dust may be replenished by weak inflow

onto the protoplanetary disk (Dominik and Dullemond 2008), by viscous mixing from outside the “dead-zone” (Birnstiel et al. 2008), or by collisional grinding; in addition, main belt asteroids do not constitute a fossil record of the first generation of planetesimals. The degree of activity in the “dead-zone” remains to be clarified (Turner et al. 2007; Bai and Goodman 2009), but there is general agreement in the literature that disk quiescence facilitates planetesimal formation (e.g., Youdin and Shu 2002; Cuzzi and Weidenschilling 2006). Since the protoplanetary disk may remain turbulent and variable during its initial stages (the “FU-Ori” epoch) lasting a few  $10^5$  years (Bell et al. 2000), we take  $\lesssim 10^6$  years to be the planetesimal formation timescale, implying that these planetary building blocks incorporate significant quantities of short-lived radioactive elements.

In Sec. 2 we discuss the framework and model parameters for the computation of the mass delivery to the circumplanetary disk. In Sec. 3 we describe the compositional constraints that our model seeks to address, and the physical processes used to that end. We briefly discuss the thermal evolution of planetesimals in the Jupiter-Saturn region due to the presence of SLRIs in Sec. 4. We close with our conclusions in Sec. 5.

## 2 Model parameters

Following giant planet formation planetesimals in its feeding zone undergo collisional grinding. In the Jupiter-Saturn region the collisional timescale for kilometer-sized objects is similar to the ejection timescale  $\sim 10^4$  yrs, so that a fraction of the mass of solids will be fragmented into objects smaller than 1 km (Stern and Weissman 2001; Charnoz and Morbidelli 2003). The collisional cascade facilitates planetesimal delivery to the circumplanetary disk because smaller planetesimals are easier to capture. An estimate of the size that will be fragmented may be obtained by equating the ejection time  $\tau_{eject} \sim 0.1 \Omega^{-1} (M_\odot/M_P)^2$ , where  $\Omega$  is the angular velocity,  $M_P$  is the planet’s mass and  $M_\odot$  is the Sun’s mass, to the collision time  $\tau_s \sim \rho_s r / \Omega \sigma_s$ , where  $\rho_s$  is the density of the solids,  $r$  is the particle size and  $\sigma_s$  is the surface density of the solids. This yields particles as large as 10 km at Jupiter (and larger for Saturn) for surface densities a few times the minimum mass (Hayashi 1981).

Switching to the subnebula, in the SEMM model (MEa,b) one expects a factor of  $\sim 10$  enhancement in solids over cosmic mixtures, resulting in a gas surface density of  $\sim 10^4$  g cm $^{-2}$  (see Sec. 2.2), which is consistent with and quantitatively constrained by the gap-opening condition for Ganymede and Titan in a inviscid disk with aspect ratio  $\sim 0.1$  (Rafikov 2002; MEb), and the Type I migration of full-sized satellites in such a disk (MEb; Bate *et al.* 2003). If we use a gas surface density of  $10^4 - 10^5$  g cm $^{-2}$  for the Jovian and Saturnian subnebulae, then a planetesimal of density  $\sim 1$  g cm $^{-2}$  will encounter a gas column equal to its mass if its radius is in the range 0.1 – 1 km, resulting in ablation and delivery to the circumplanetary disk.

Our aim here is to provide a link via ablation of planetesimal fragments in the Jupiter-Saturn dynamically active region to the circumplanetary disks of these two planets, seeking to account for the mass and angular momentum budgets and compositions of the regular satellites. Tying solar nebula planetesimals to subnebula satellites involves three different aspects: first, characterizing the properties of the first generation of planetesimals in

terms of sizes and degree of heterogeneity; second, quantifying the collisional evolution of the planetesimal swarm following giant planet formation; and third, delivering planetesimal fragments to the circumplanetary disks of Jupiter and Saturn.

## 2.1 Planetesimal fragmentation and the initial size distribution

The strength of planetesimals is an unknown quantity. A strain-rate scaling law by Housen *et al.* (1991) suggests that kilometer-sized objects are the weakest. Davis and Farinella (1997) find a constant  $S = 3 \times 10^6$  erg cm<sup>-3</sup>, where  $S$  is the impact strength (*i.e.*, the energy per unit volume for shattering fifty percent by mass of the parent body) for crushed icy bodies, in agreement with Ryan *et al.* (1999). Benz and Asphaug (1999) use a 3D Hydrocode to simulate 3 km/s impacts and find that 100 m objects may be weakest, with kilometer sized planetesimals strengthened by gravity. How much planetesimal mass fragments following the collisional cascade and is delivered depends on the planetesimal strength (Charnoz and Morbidelli 2003).

The initial size distribution is also unknown. If run-away growth takes place the resulting size distribution may be steep. Wetherill and Stewart (1993) find a bimodal size distribution with a fragmentation tail of objects less than 1 km with power law exponent  $q \sim 3.5$  and size distribution for objects larger than that with  $q \sim 5.5$ , where the differential size distribution ( $dN/dr \propto r^{-q}$ ) approaches a value of  $q \sim 3.5$  in the case of a size independent fragmentation model (e.g., Dohnanyi 1969). In his coagulation simulations Weidenschilling (1997) finds that most of the mass resides in objects  $\sim 10$  km in a timescale of  $10^5 - 10^6$  years in the outer nebula. Most studies of planet formation start with most of the mass of solids in objects of size  $\sim 10$  km, as suggested by numerical simulations (e.g., Kenyon and Luu 1999).

Unless otherwise stated, we consider values of  $q = 3.5$ . We set the lower size cut-off at 1 m. The reason is that smaller objects are protected from further collisional grinding by gas drag, so that below this size collisions are once again accretive as long as the nebula turbulence is weak. We vary the upper size cut-off between 10 – 100 km *in lieu* of more detailed collisional fragmentation simulations, which we leave for further work. For simplicity, we also assume a fully fractionated population of icy and rocky (which includes iron) planetesimal fragments, each of which has the same particle size spectrum (see Sec. 4).

## 2.2 Disk properties

Gas flowing into its Hill sphere forms a disk around the protoplanet. The timescale for Jupiter and Saturn to clear a gap in between  $\sim 10^4$  years sets the time for the end of gas accretion. The timescale for envelope collapse is given by the Kelvin-Helmholtz time of  $10^4 - 10^5$  years (Hubickyj *et al.* 2005), following which a circumplanetary disk forms. *Prior* to gap-opening the giant planet accretes gas with semi-major axis originating from  $\sim R_H$  of its location, where  $R_H = a(M_P/3M_\odot)^{1/3}$  is the planet’s Hill radius, centrifugal balance yields a characteristic disk size of  $\sim R_H/50$  (Stevenson *et al.* 1986; MEa). For Jupiter and Saturn these radii are located close to the positions of Ganymede and Titan. *After* gap-opening accretion continues through the planetary Lagrange points, and the estimated characteristic disk size is larger  $\sim R_H/5$  (MEa; Estrada *et al.* 2009; Ayliffe and Bate 2009), which we take



to be the radial extent of the circumplanetary disk. This radial size corresponds to  $\sim 150 R_J$ , and  $\sim 200 R_S$ , where  $R_J$  and  $R_S$  are the radii of Jupiter and Saturn, respectively.

MEa divide the circumplanetary disk into inner and outer regions. For Jupiter, we compute the solids-enhanced minimum mass (SEMM) gas densities in the inner and outer disks based on the solid mass required to form Io, Europa (both re-constituted for missing volatiles) and Ganymede in the inner disk, and Callisto in the outer disk. Inside of the centrifugal radius the surface gas density is  $\Sigma \sim 10^4 - 10^5 \text{ g cm}^{-2}$ , which corresponds to pressures  $\sim 0.1 \text{ bar}$ . Outside the centrifugal radius  $R_c \sim 30 R_J$ , the gas surface densities are in the range  $10^2 - 10^3 \text{ g cm}^{-2}$ . We apply the same procedure to the circumplanetary disk of Saturn by employing the masses of Titan and Iapetus to set the inner and outer disk masses, respectively. The transition region has a width  $\gtrsim 2H_c$ , where  $H_c$  is the subnebula scale-height at the centrifugal radius. This choice ensures that the gradient in gas density is not so steep as to lead to a Rayleigh-Taylor instability (e.g., Lin and Papaloizou 1993).

The subnebula gas surface density profile is taken to be

$$\Sigma(R) = \begin{cases} \Sigma_a(R_a/R), & R < R_a; \\ \Sigma_a(R_a/R) - \frac{\Sigma_a(R_a/R) - \Sigma_b(R_b/R)^2}{e^{\frac{R_a+R_b-R}{2n}} + 1}, & R_a < R < R_b; \\ \Sigma_b(R_b/R)^2, & R > R_b. \end{cases} \quad (1)$$

Once a disk forms, the cooling timescale depends on the opacity. As particles grow, the opacity of the nebula decreases, allowing the gas to cool and accretion of ice-rich satellites to take place. We connect the disk's temperature profile to the planetary luminosity at the tail end of giant planet formation (Hubickyj *et al.* 2005). We use a heuristic temperature profile of the form  $T = 3600 R_J/R$  for Jupiter (e.g., Lunine and Stevenson 1982) and  $T = 2000 R_S/R$  for Saturn. The outer disks of Jupiter and Saturn have roughly constant temperatures in the range of 70 – 130 K for Jupiter and 40 – 90 K for Saturn, depending on solar nebula parameters.

### 3 Regular Satellite Mass and Composition Constraints

The compositional gradient of the Galilean satellites may provide a probe to the environment in which they formed (Estrada *et al.* 2009 and references therein). Here we focus on the large, outer regular satellites of each satellite system: Ganymede and Callisto in the case of Jupiter; and Titan and Iapetus for Saturn. Planetesimal break-up in tandem with delivery via ablation of planetesimal fragments crossing the subdisk provides a framework for understanding the mass budget and compositions of regular satellites compared to that of solar nebula planetesimals.

#### 3.1 Thermal Ablation of Disk Crossers

Thermal ablation occurs because friction of the fast moving heliocentric interloper as it crosses the circumplanetary gas disk heats up the body. At low gas densities impactors lose

mass and energy through ablation. For large kilometer-sized bolides mechanical destruction rather than thermal ablation may dictate the fate of the object (e.g., Zahnle and Mac Low 1994). Ablation of planetesimal fragments < 1 km may deliver the bulk of the solids needed to form the satellites. For objects in that size range, the heat transfer coefficient  $C_H \sim 0.1$  may be reasonably obtained from observations of terrestrial meteorites (Bronshten 1983). The rate at which energy is transferred to the planetesimal per unit area is given by  $E \sim 0.5C_H\rho v^3$ , where  $\rho$  is the gas density,  $v$  is the speed of the planetesimal through the gas, and some planetesimal flattening (which increases its cross section) takes place (e.g., Zahnle 1992; Chyba *et al.* 1993). Ablation thus results in delivery of material to the circumplanetary disk. Gas drag can also result in capture of material.

Ignoring conduction into the interior and ablation, we can obtain the surface temperature  $T_{surf}$  by balancing this heating and radiative cooling  $\epsilon\sigma_{SB}T_{surf}^4$ ,

$$T_{surf} = \frac{1}{\epsilon^{1/4}} \left( \frac{fC_H}{8\sigma_{SB}}\rho v^3 + T_0^4 \right)^{1/4}, \quad (2)$$

where  $\epsilon = 0.5$  is the emissivity,  $T_0$  is the subnebula background temperature,  $\sigma_{SB}$  is the Stefan-Boltzmann constant,  $v$  is the speed of the planetesimal through the gas disk, and  $f$  is a parameter that measures the degree of flattening. It is important to keep in mind that this quantity reflects the energy regime not the actual surface temperature unless it is low enough that ablation can be ignored. Using parameters appropriate at the location of Iapetus  $v \sim 5 \times 10^5$  cm s<sup>-1</sup> (a cold population at infinity),  $f = 4$  and  $\rho = \Sigma/2H \sim 7 \times 10^{-10}$  g cm<sup>-3</sup>, where  $\Sigma$  is the gas surface density and  $H = c/\Omega$  is the scale-height,  $c$  the sound speed and  $\Omega = \sqrt{GM_P/R^3}$  is the angular velocity in the circumplanetary disk, we obtain a surface temperature of  $T_{surf} \sim 900^\circ$  K, which is sufficient to melt and vaporize icy objects but not rocky objects. A value of  $f = 1$ , which is suitable to the outer disk due to the low ram pressures there, yields a temperature of  $\sim 600^\circ$  K. In contrast, at Titan ( $v \sim 8 \times 10^5$  cm s<sup>-1</sup>;  $\rho \sim 3 \times 10^{-7}$  g cm<sup>-3</sup>) and Callisto ( $v \sim 1.1 \times 10^6$  cm s<sup>-1</sup>;  $\rho \sim 2 \times 10^{-7}$  g cm<sup>-3</sup>) the surface temperature can exceed  $4000^\circ$  K (for  $f = 4$ ), which is enough to melt and vaporize rocky objects as well. Hence, the temperature of objects crossing the disk places Iapetus in a separate regime from other regular satellites, i.e., at its location in the disk rocky objects do not reach temperatures high enough to ablate.

We can estimate the change in radius of an icy planetesimal due to either melting or vaporization as it crosses the gas disk in a time  $\Delta t \approx 2H/v$  (ignoring gas drag for now) (Podolak *et al.* 1988)

$$\left( \frac{dr}{dt} \right)_{vap,melt} \approx -\frac{fC_H\rho v^3}{8\rho_p E_{0c,m}} \left\{ 1 - \frac{8\sigma_{SB}T_0^4}{fC_H\rho v^3} [\epsilon(T_{c,m}/T_0)^4 - 1] \right\}, \quad (3)$$

where  $\rho_p$  is the planetesimal density,  $T_c = 648^\circ$  K is the critical temperature for vaporization, and  $T_m = 273^\circ$  K is the melting temperature.  $E_{0m} = 6.0 \times 10^9$  erg g<sup>-1</sup> is the energy required to raise the temperature of 1 g of ice from the background temperature of the nebula  $\sim 100^\circ$  K (where it originated) to  $T_m$  plus the latent heat of melting  $H_f$ , and  $E_{0c} = 2.8 \times 10^{10}$  erg g<sup>-1</sup> is the energy needed to raise the temperature of 1 g of icy material for  $100^\circ$  K to  $T_c$  (so that vaporization becomes energy limited) plus the latent heat of vaporization  $H_v$ . We find

that the amount of ice melted or vaporized at Iapetus ( $\Delta t \sim 3 \times 10^5$  s) is in the order of meters (for  $f = 1$ ), whereas at Titan and Callisto ( $\Delta t \sim 4 \times 10^4$  s) it is about a kilometer (for  $f = 4$ ). It should be noted that at Iapetus ( $\Sigma \sim 100$  g cm $^{-2}$ ) meter-sized objects (with density  $\sim 1$  g cm $^{-3}$ ) traverse a column of gas equal to their mass, whereas at Titan and Callisto ( $\Sigma \sim 10^4$  g cm $^{-2}$ ) the same is true for kilometer-sized objects. Hence, ablation of planetesimal fragments may provide the solids needed for the formation of the regular satellites provided that a significant fraction of the planetesimal mass resides in fragments with sizes in the kilometer to meter size range.

One can ask whether a particle will ablate versus breakup when crossing the disk. At Titan, the dynamic pressure is  $P_{dyn} = \rho v^2/2 \sim 10^5$  dynes cm $^{-2}$ . At Iapetus, we find  $P_{dyn} \sim 100$  dynes cm $^{-2}$ . Therefore, if a meter-sized or larger particle with strength  $S \sim 10^6$  dynes cm $^{-2}$  crosses the disk icy material is left behind by ablation (at Titan and Iapetus) or by gas drag capture (at Titan), but probably not breakup (at least at Iapetus). It is also important to consider the sensitivity of our results to the flattening parameter  $f$ . In this regard, it should be noted that the overall dependence of ablation on  $f$  is not too strong, and that at the location of Iapetus the ram pressure is low enough that  $f = 1$  is a good approximation.

To find out the mass budget and composition of the subnebula resulting from the ablation of an unmixed population of rocky and icy disk crossers, we have to tackle the thorny issue of whether the rate of ablation in Eq. 3 is dominated by melting or vaporization. It is probably fair to say that most models of the ablation process focus on vaporization (e.g., Moses 1992). However, at lower temperatures the rate of ablation may be affected by the viscosity of the melt and other factors (see Podolak et al. 1988 for a discussion). Yet, a detailed model incorporating the full complexity of the problem for a broad range of parameter space is premature in that it can obscure our conclusions. In fact, as we show below, our main results are robust and not dependent on the specifics of the ablation mechanism. For this reason, we leave development of a more detailed ablation model for later work, and we employ the classic approach of Bronshten with minor modifications. We calculate the amount of material ablated by solving coupled equations of motion and ablation (Bronshten 1983) for a planetesimal of mass  $m$  which is assumed for simplicity to cross the circumplanetary disk perpendicular to the disk plane:

$$m \frac{dv}{dt} = -\frac{1}{2} C_D A(m) \rho(X, Z) v^2 - m \Omega^2(X) z; \quad (4)$$

$$\frac{dm}{dt} = -\frac{C_H}{2E_{0c,m}} A(m) \left[ \rho(X, Z) v^3 - \frac{8\sigma_{SB}}{C_H} (\epsilon T_{c,m}^4 - T_0^4) \right] \text{ for } T_{surf} > T_{c,m}; \quad (5)$$

$$\frac{dm}{dt} = 0 \text{ for } T_{surf} \leq T_{c,m},$$

where  $T_{surf}$  is obtained from Eq. 2 with  $f = 1$ ,  $C_D = 0.44$  is the drag coefficient,  $A$  is the planetesimal cross-section,  $X = R/R_P$  is the distance from the planet in units of planetary radii  $R_P$ ,  $Z = z/\sqrt{2}H$ ,  $\rho(X, Z) = \rho_0(X)e^{-Z^2}$  is the gas density of the subnebula. Here we set the flattening factor  $f = 1$  because we are particularly interested in the outer disk, where

the ram pressure is low. Note that for  $T_{surf} \leq T_{c,m}$  the ablation equation goes to zero even though the planetesimal can still be captured by gas drag. That is, regions of the disk such that the disk crosser never reaches the ablation temperature  $T_{c,m}$  may only be delivered to the circumplanetary disk by gas drag capture. Fits to observational data of meteoroids in the atmosphere yield values of  $C_H \simeq 0.1$  for low values of the effective heat of ablation  $\sim 10^{10}$  erg g<sup>-1</sup> (Svetsov et al. 1995), which leads us to use  $E_{0m} = 3.0 \times 10^{10}$  erg g<sup>-1</sup> and an ablation temperature of  $T_m = 1800^\circ$  K for rock. For ice we consider both melting ( $E_{0m} = 6.0 \times 10^9$  erg g<sup>-1</sup>;  $T_m = 273^\circ$  K) and vaporization ( $E_{0c} = 2.8 \times 10^{10}$  erg g<sup>-1</sup>;  $T_c = 648^\circ$  K) while keeping  $C_H \simeq 0.1$  constant. We stress that these parameter choices are quite conservative and intended to test the sensitivity of our results, as significant water-ice sublimation will take place for  $T_{surf} < T_{c,m}$ . Thus, a more realistic treatment is likely to deliver significantly more water to the outer disk.

We solve Equations 4 and 5 using a fourth order Runge-Kutta scheme for coupled equations. In Fig. 1 we plot final velocity relative to initial  $v_{final}/v_{init}$ , final planetesimal size  $r_{final}$ , distance travelled through the disk  $z/H$ , and delivered mass fraction due to ablation and gas drag capture as a function of the distance from Jupiter,  $X$ , for different particle sizes. Here the gas surface density corresponds to that of a SEMM model  $\Sigma(X) = 3 \times 10^5 / X$  g cm<sup>-2</sup> (without a transition). These results use the more conservative ice vaporization values for the ablation temperature  $T_c$  and heat of ablation  $E_{0c}$ . If the planetesimal does not completely ablate, it may successfully pass through the disk. However, planetesimals may fail to traverse the disk because they are ablated before they do, or because of gas drag capture. If particles are ablated down to a size of 1 cm, they are taken to have totally ablated. Close to the planet even  $\sim 1$  km planetesimals (bold solid lines) are completely ablated before reaching a final velocity  $v_{final} = 0$  (top left panel). Farther out in the disk, a leftover planetesimal of size  $r_{final}$  (top right panel) emerges from the disk after crossing a distance of  $2H$  (bottom left panel). As expected, the mass delivered to the disk by either capture or ablation decreases with distance from the planet (bottom right panel).

In the top left curve of Fig. 1 we also plot the escape velocity  $v_{esc} = \sqrt{2GM_P/(R_P X)}$  as function of distance (light solid line) for reference. It is important to point out that here (and in the rest of this paper) our capture condition is defined locally. That is, we only consider that the particle has been *locally* captured if  $v_{final} = 0$ . A planetesimal can emerge from the disk with a speed too slow to escape the gravitational potential well of the planet, so that it will be delivered either to the circumplanetary disk or the planet. For instance, 10 m particles (short dashed lines) have final speeds that are less than the escape speed out to the edge of the disk. Therefore, these particles will be delivered to the circumplanetary disk, but not always *locally*. Here we require  $v_{final} = 0$  for capture since in this case the planetesimal mass is delivered at the location of passage. This is conservative in the sense that it underestimates the mass delivered to the circumplanetary disk. But it is likely to provide a better estimate of the ice/rock ratio as a function of position because particles with significant non-zero exit velocities can potentially be delivered anywhere inside the crossing radius. We leave a more realistic treatment of multiple passes through the disk for later work.

In Fig. 2 we do the corresponding calculations for the case of rock. Note that in the case of rock we employ the rock melting values for the ablation temperature  $T_m$  and heat of ablation

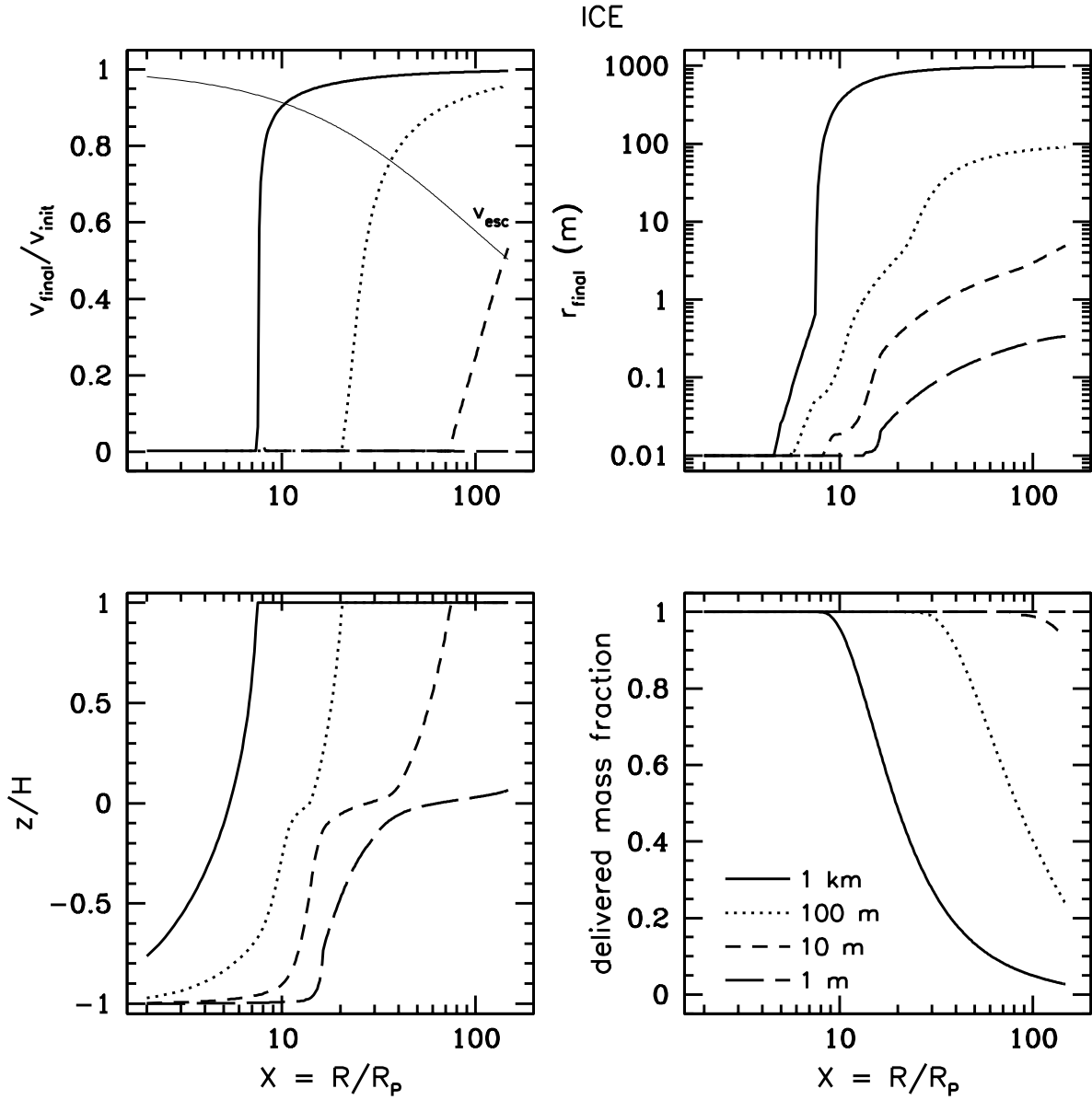


Figure 1: Plot final velocity relative to initial  $v_{final}/v_{init}$ , final planetesimal size  $r_{final}$ , distance travelled through the disk  $z/H$ , and delivered mass fraction due to ablation and gas drag capture as a function of the distance from Jupiter,  $X$ , for several initial planetesimal sizes (indicated by the solid and dashed curves). The gas surface density is taken to be that of the SEMM model,  $\Sigma(X) = 3 \times 10^5/X \text{ g cm}^{-2}$  (without a transition). We take the initial velocity as the interloper crosses the disk to be  $v_0 \approx 60/\sqrt{X} \text{ km s}^{-1}$ . The planet's escape velocity as a function of distance  $v_{esc}$  is plotted in the top left panel.

$E_{0m}$ . For rock the mass delivered for a given particle size (bottom right panel) drops faster than for ice despite our conservative choice of parameters for ice ablation. Consequently, the composition of disk is expected to be enriched in ice. Rock mass delivery in the outer

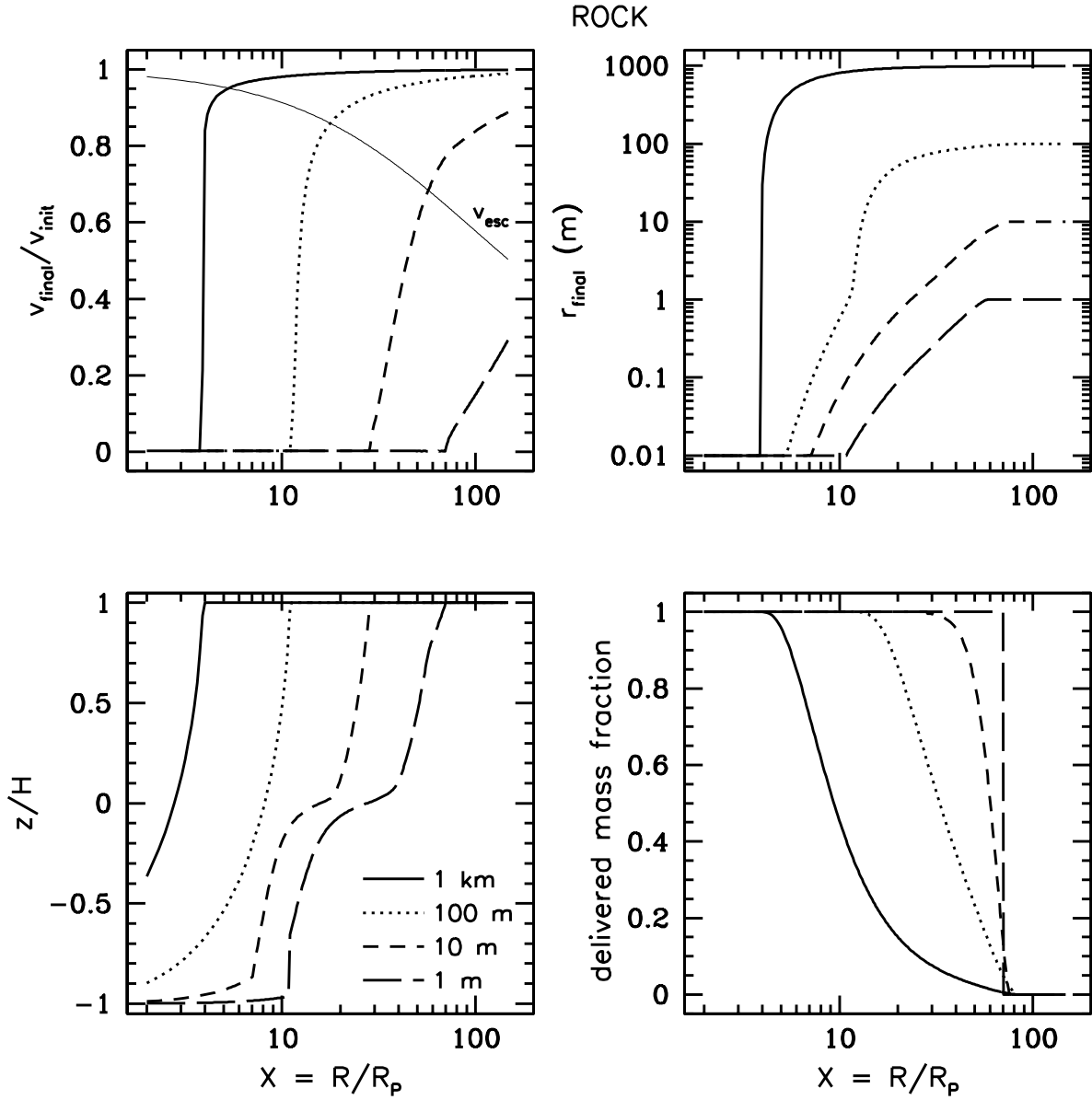


Figure 2: Plot final velocity relative to initial  $v_{final}/v_{init}$ , final planetesimal size  $r_{final}$ , distance travelled through the disk  $z/H$ , and delivered mass fraction due to ablation and gas drag capture as a function of the distance from Jupiter,  $X$ , for several initial planetesimal sizes (indicated by the solid and dashed curves). The gas surface density is taken to be that of the SEMM model,  $\Sigma(X) = 3 \times 10^5/X \text{ g cm}^{-2}$  (without a transition). The planet's escape velocity as a function of distance  $v_{esc}$  is plotted in the top left panel.

disk can be dominated by capture. This can be seen by the behavior of 1 m particles (long dashed lines): gas drag slows down these particles sufficiently fast that almost no ablation takes place beyond  $X = 60$  so that  $r_{final} = 1 \text{ m}$  (top right panel). Yet gas drag is effective out to  $X = 70$  despite the low surface density of the outer disk so that  $v_{final} = 0$  (top

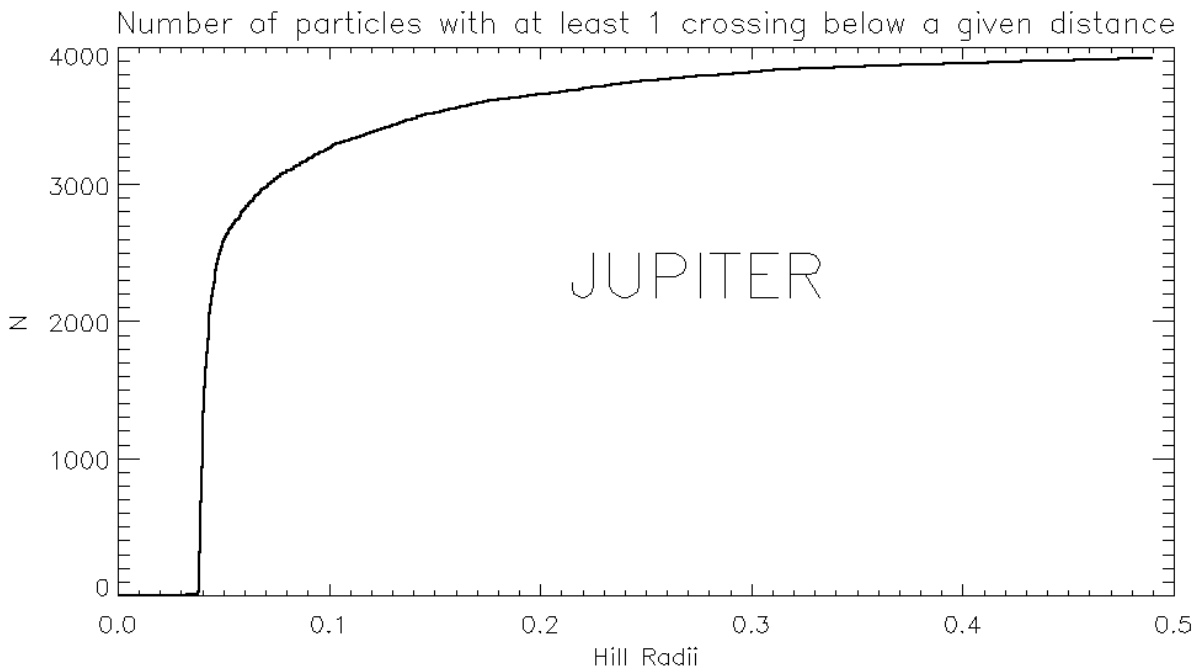


Figure 3: Number of particles with at least one crossing inside a given distance from Jupiter. Simulations involved 5000 particles with total mass of  $10 M_{\oplus}$ . We estimate that roughly  $\sim 7 M_{\oplus}$  pass within  $0.2 R_H$ .

left panel) and the full particle mass is delivered by gas drag capture out to this location (bottom right panel). Outside this location essentially no rock is delivered. Because ice is still ablated and captured outside this location (Fig. 1), one can expect the cold outer disk to be water-ice enriched following re-condensation.

We follow the dynamical evolution of a  $10 M_{\oplus}$  mass disk (where  $M_{\oplus}$  is an Earth mass) of 5000 particles spread between 4 and 8 AU starting on low eccentricity and inclination orbits. Jupiter is placed at 5 AU and Saturn is at 7.5 AU (packed configuration), both with low values of eccentricity and inclination. In Figures 3 and 4 we plot the number of particles that crossed at least once within a given distance of Jupiter and Saturn in  $10^5$  years. Not surprisingly, a large fraction of the total number of particles in the simulation (5000) cross at least once within 0.1 of the Hill sphere of Jupiter or Saturn in the first  $\sim 10^4$  yrs. This is because particles are scattered during close encounters with the giant planets. Several caveats apply to these results. For one, collisional fragments, which are easier to deliver to the circumplanetary disk, may collide frequently, which would change their dynamics. This process is not modeled in the results discussed above, and is left for future work. But we stress that collisions cannot prevent collisional debris from crossing the circumplanetary disk of either giant planet – particles of any size at the gap edge and beyond are able to penetrate the Hill sphere of the giant planet during close encounters. In some regimes of interest, such as cases in which nebula gas drag and collisional damping is included and meter-sized particles play an important role, one needs to treat the full fragmentation-coagulation problem. However, it is presently unclear how much mass the tail

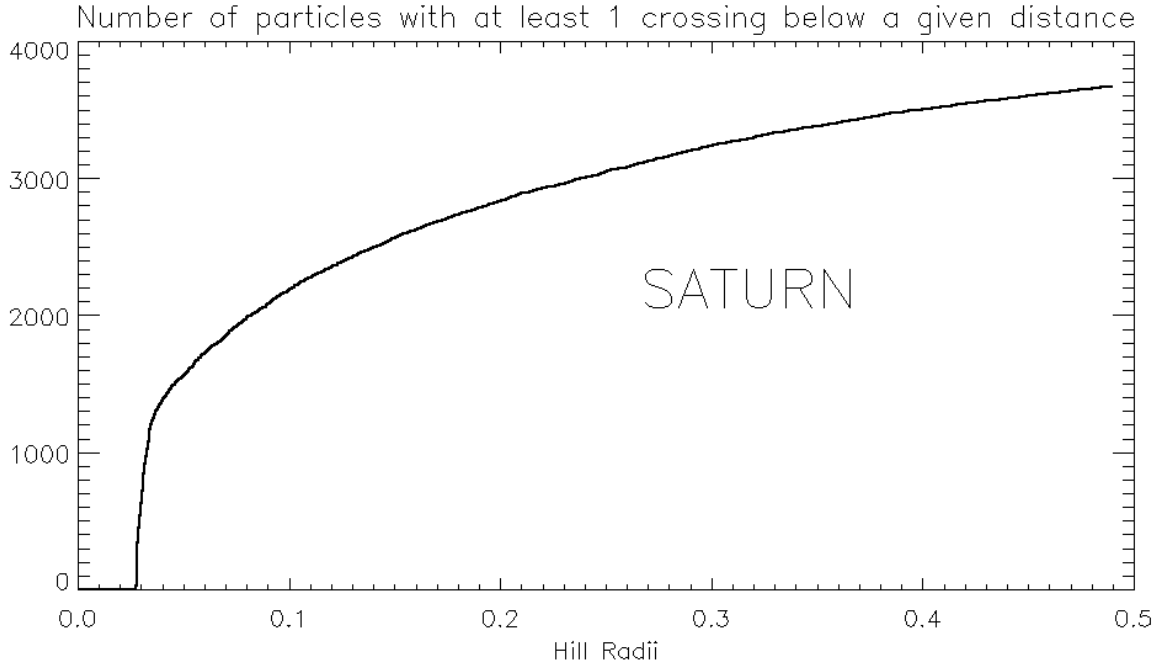


Figure 4: Number of particles with at least one crossing inside a given distance from Saturn. Simulations involved 5000 particles with total mass of  $10 M_{\oplus}$ . We estimate that roughly  $\sim 5 M_{\oplus}$  pass within  $0.2 R_H$ .

end of the mass-spectrum contains.

We calculate the total captured mass of the ice and rock components  $M_j(X)$  delivered within a radius  $X = R/R_P$  to the circumplanetary disk in time  $\tau$  using (e.g., Estrada and Mosqueira 2006)

$$M_j(X) = 2\pi\tau R_P^2 \int_1^X F_j(X') X' dX';$$

$$F_j(X) = v_0(1 + l\Theta/X) \int_{m_{min,j}}^{m_{max,j}} c_j \Phi_j(X, m) m^{1-p} dm, \quad (6)$$

where  $F_j$  is mass inflow deposition rate per unit area of component  $j$ ,  $v_0$  is the speed at infinity,  $p = (1/3)(q + 2)$ ,  $m_{min,j}$  and  $m_{max,j}$  are the lower and upper bounds of the mass distribution of component  $j$ ,  $\Theta = GM_P/R_P v_0^2$  is the Safronov parameter,  $l \sim 1 - 2$  is a constant, and  $\Phi_j(X, m)$  is the fraction of a planetesimal with mass  $m$  that is delivered to the disk at  $X$ , as obtained from Eqs. 4 and 5. The  $c_j$  are normalization coefficients given by

$$c_j = \frac{(2-p)M_{pl}}{2\pi R_P^2 v_0 \tau} \left[ \frac{1}{2}(X_D^2 - 1) + l\Theta(X_D - 1) \right]^{-1} \times \begin{cases} \frac{1-x_r}{m_{max,i}^{2-p} - m_{min,i}^{2-p}} & \text{for ice;} \\ \frac{x_r}{m_{max,r}^{2-p} - m_{min,r}^{2-p}} & \text{for rock} \end{cases}, \quad (7)$$



where  $M_{pl}$  is the mass of planetesimals passing through the disk,  $x_r$  is the mass fraction of rock, and for our disk size we take  $X_D = 0.2R_H/R_P$ . The surface density of components  $j$ ,  $\Sigma_j$ , solids-to-gas-ratio, and the ice mass fraction as a function of radius are obtained from the  $F_j(X)$ .

Pending more detailed scattering/fragmentation simulations, we assume a power-law mass distribution with slope  $q = 3.5$  and an upper and lower particle size cut-offs of  $r_{max} = (3m_{max}/4\pi\rho_p)^{1/3} = 200$  km and  $r_{min} = (3m_{min}/4\pi\rho_p)^{1/3} = 0.001$  km for both rock and ice. We allow for a differentiated population of icy and rocky fragments with a 30/70 ratio by mass. Based on our  $N$ -body simulations, we estimate that about  $M_{pl} \sim 7 M_\oplus$  cross at least once within  $0.2 R_H$ . It should be noted that particles  $\sim 1$  km that cross the disk at  $\gtrsim 0.1 R_H$  are not in general ablated so they may cross again within  $0.2 R_H$  before being ejected. We take the Safronov parameter  $\Theta = 25$  representative of a fairly cold population. The factor  $l$  accounts for the different geometry of a flux of impactors through the subnebula rather than the planet itself (Morfill et al. 1983; Cuzzi and Estrada 1998; Charnoz et al. 2009). The value for  $l$  should be obtained from numerical simulations. For now we use  $l = 2$ , but the results are not sensitive to this parameter. The background nebula temperature is set to 130 K. For our subnebula parameters, we choose  $\Sigma_a = 2 \times 10^4$  g cm $^{-2}$ ,  $\Sigma_b = 5 \times 10^3$  g cm $^{-2}$ ,  $R_a = 15 R_J$ ,  $R_b = 25 R_J$ , and  $n = 1$ . The velocity of the planetesimal is given by  $v = \sqrt{v_0^2 + v_{esc}^2}$ .

In Fig. 5 we show the mass delivery by ablation and gas drag capture of planetesimal fragments crossing the SEMM circumplanetary disk. The top left panel indicates the size of the largest particle that will be delivered to the disk in full by a combination of ablation and capture of the leftover object (dotted curves). It can be seen that a higher proportion of mass is delivered by capture for rock than for ice (especially for the ice melt curve). This is because less ablation makes the rock particle cross section and gas drag force larger for a given size. The top right panel corresponds to the solids/gas fraction that results from a cold population of planetesimal fragments as a function of position in the disk. The surface gas density is also indicated. Both the dotted and the dashed curves exhibit a bump during the inner to outer disk transition. This jump in the concentration of solids occurs because in the transition region the surface gas density of the disk decreases faster than the decrease in the mass delivery. Consequently, the concentration of solids increases. The subsequent outer disk rise in the dotted curve and bump in the dashed curve are related to the  $1/R^2$  surface density profile in the outer disk (compared to a  $1/R$  profile in the inner disk) together with the transition to an isothermal temperature profile in the outer disk (compared to a  $1/R$  profile in the inner disk). The dashed curve drops towards the outer edge because the temperature of the planetesimal becomes too low for significant vaporization either of rock or ice (whereas the temperature is still high enough to melt water-ice). The bump in the concentration of solids at the transition between the inner and outer disk is tantalizing in that it can help to accrete satellites close to the present location of Ganymede (and Titan for Saturn's disk). But it is premature to say that this feature is significant. The bottom left panel indicates the resulting ice/rock fraction of the disk. The bottom right panel indicates the total mass delivered within a radial distance  $R$ . The region between the bars contain enough mass to make each of the indicated satellites (reconstituted in the case of Io and Europa). The mass delivered was obtained by using the ice melt results for  $T_{surf} < T_c$  and the vaporization

results for larger  $T_{surf}$ . These results indicate that enough mass can be delivered to account for the reconstituted Galilean satellites. But we stress that the mass delivered to the disk is dependent on the parameters chosen and the capture condition  $v_{final} = 0$ . On the other hand, the capture condition is a conservative choice in that significantly more mass will be delivered to the circumplanetary disk than we assume here. We reserve a parameter study for later work.

The two ice curves shown correspond to ablation by melting and vaporization in Eq. 5. As one would expect, more ice is delivered when ablation turns on at the lower temperature of melting  $T_m$  versus vaporization  $T_c$ . The good agreement with the mass budget and compositions of Ganymede and Callisto would appear to argue in favor of the vaporization curves. However, this conclusion is premature for several reasons. First, these calculations make the assumption that the population of disk crossers is completely fractionated, which is unrealistic even if primordial planetesimals were fully differentiated (see Sec. 4), as some mixing would be expected during collisional disruption. A more realistic treatment would lower the ice/rock ratio of the entire disk. Two, vaporization of water-ice actually starts below the melting temperature  $T_m = 273^\circ$  K (whereas for rock temperatures  $200^\circ$  K above melting  $T_m = 1800^\circ$  K are needed before significant vaporization takes place; Podolak et al. 1988). Third, the total mass delivered to the circumplanetary disk is dependent on parameter choices. However, the result that the outer disk is icier than the inner disk is independent of the specifics of the ablation model. In fact, given a fully fractionated population crossers, the outer disk receives material mostly by ablation of ice, and essentially no rock either by ablation or capture. Also, these results lead one to expect that the circumplanetary disk is enriched in ice over solar mixtures for a broad range of parameter choices.

Similarly for Saturn, we assume a power-law mass distribution with slope  $q = 3.5$  and allow for a differentiated population of icy and rocky fragments with a 30/70 ratio by mass. Based on our simulations, we estimate that about  $M_{pl} \sim 5 M_\oplus$  cross at least once within  $0.2 R_H$  of Saturn. We let  $\Theta = 100$  and an upper and lower particle size-cutoffs of  $r_{max} = 50$  km and  $r_{min} = 0.001$  km for both rock and ice based on the larger fraction of rubble and lower velocity dispersion expected for Saturn. The background nebula temperature is set to 90 K. For our subnebula parameters, we chose  $\Sigma_a = 2 \times 10^4$  g cm $^{-2}$ ,  $\Sigma_b = 2 \times 10^3$  g cm $^{-2}$ ,  $R_a = 20 R_S$ ,  $R_b = 58 R_S$ , and  $n = 3$ . As we can see from Fig. 6, rocky fragments in the 0.001 – 1 km are not either captured or ablated, whereas icy fragments are delivered mostly by ablation. Thus, delivery of solids via ablation of a non-homogeneous population of planetesimal fragments leads to an enrichment of water-ice in Saturn’s outer disk.

In summary, these results show that it is possible to deliver enough mass to account for the regular satellites of Jupiter and Saturn. Furthermore, ablation and the capture cross-section of meter-sized objects can lead to ice/rock fractionation and account for the composition of Iapetus, as well as those of Ganymede, Callisto and Titan. This is the only explanation currently available for Iapetus’ icy composition, and may also indicate that regular satellites overall may be depleted in rock with respect to solar composition mixtures, which might explain why their densities are lower than that of similar size Kuiper belt objects. We stress that while the amount of mass delivered to the circumplanetary disks of Jupiter and Saturn is dependent on parameter choices, such as the upper size cut-off and the slope of the mass spectrum, the velocity dispersion at infinity and the capture condition, we found that the

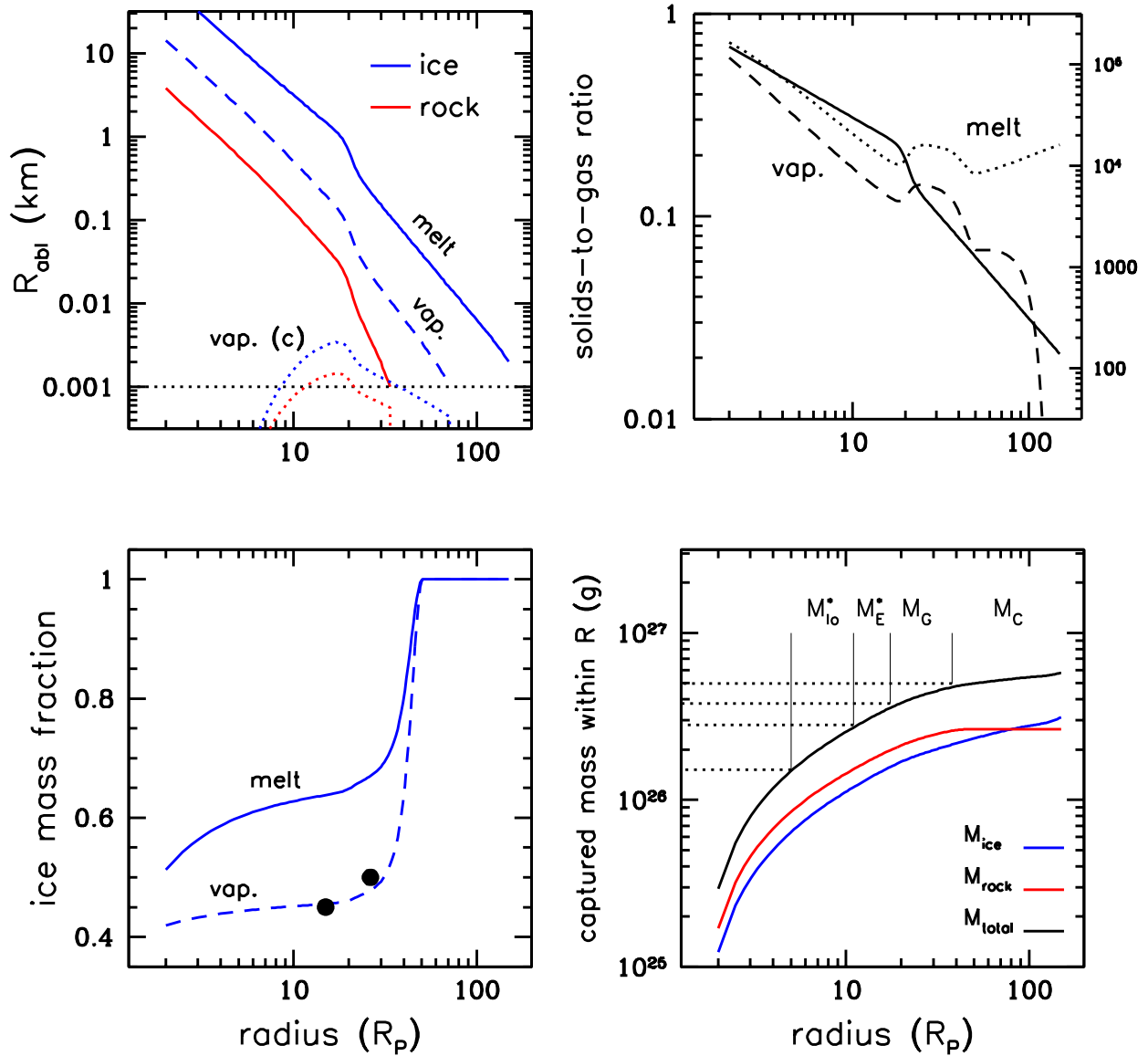


Figure 5: Left upper panel: The planetesimal size that gets ablated (solid and dashed curves) and captured (dotted curves) as function of radial distance. The dotted horizontal line corresponds to the lower size cut-off. Right upper panel: The solids to gas ratio for the two ice models (dotted and dashed curves) as a function of radial distance from Jupiter. The bold solid curve indicates the gas surface density of the disk in  $\text{g cm}^{-2}$  (right side). Left lower panel: The ice to rock ratio as a function of radial distance. The solid dots correspond to Ganymede (inner disk) and Callisto (outer disk). The ice mass ratio of solar nebula planetesimal fragments crossing the disk is taken to be 0.3. Lower right panel: Plot of the mass delivered as a function of distance from Jupiter. The two models correspond to melting and vaporizing ice.

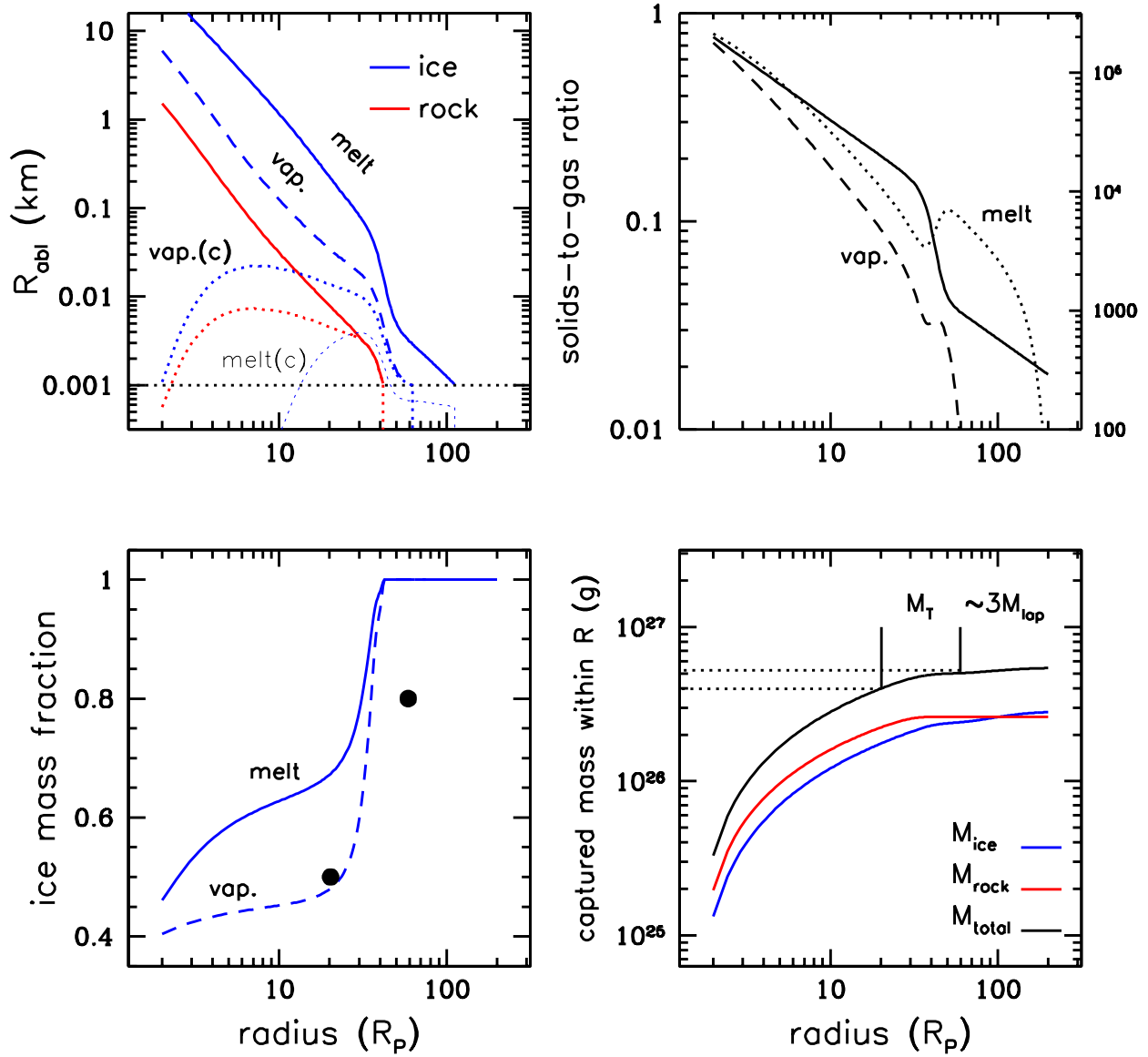


Figure 6: Left upper panel: The planetesimal size that gets ablated (solid and dashed curves) and captured (dotted curves) as function of radial distance. The dotted horizontal line corresponds to the lower size cut-off. Right upper panel: The solids to gas ratio for the two ice models (dotted and dashed curves) as a function of radial distance from Saturn. The bold solid curve indicates the gas surface density of the disk in  $\text{g cm}^{-2}$  (right side). Left lower panel: The ice to rock ratio as a function of radial distance. The solid dots correspond to Titan (inner disk) and Iapetus (outer disk). The ice mass ratio of solar nebula planetesimal fragments crossing the disk is taken to be 0.3. Lower right panel: Plot of the mass delivered as a function of distance from Saturn. The two models correspond to melting and vaporizing ice.

efficiency of delivery is high enough that the mass budget of the satellites can easily be accommodated. We find that the water-enrichment of the outer disks of Jupiter and Saturn is a robust feature given a differentiated population of icy and rocky interloper fragments.

While full ice/rock fractionation is unlikely, partial separation can account for Iapetus' icy composition. Such a population results from the fragmentation of a partially differentiated,  $^{26}\text{Al}$ -heated first generation of  $\sim 10$  km planetesimals (Mosqueira et al. 2009). Indeed, it is likely that most of the mass in the first generation of planetesimals resided in objects 10–100 km in the first  $10^5 - 10^6$  years, so that these objects incorporated significant amounts of  $^{26}\text{Al}$ , leading to partial differentiation, as we show below.

Table 1: Physical Parameters

Parameter	Ice	Rock
$\mu$ (g mole $^{-1}$ )	18	50
$\rho_s$ (g cm $^{-3}$ )	0.92	3.4
$E_{0c}$ (erg g $^{-1}$ )	$2.8 \times 10^{10}$	$8.08 \times 10^{10}$
$E_{0m}$ (erg g $^{-1}$ )	$5.94 \times 10^9$	$3.04 \times 10^{10}$
$H_f$ (erg g $^{-1}$ )	$3.33 \times 10^9$	$1.43 \times 10^{10}$
$T_m$ ( $^{\circ}\text{K}$ )	273	1800
$T_c$ ( $^{\circ}\text{K}$ )	648	4000

## 4 Differentiation of primordial planetesimals

The thermal evolution of comets (Prialnik et al. 2008) and asteroids (Ghosh et al. 2006) powered by short-lived radionuclides has been treated in an extensive number of publications, and it is not possible for us to do it justice in this brief section. Our aim here is to get a handle on the degree of differentiation of  $\sim 10$  km primordial planetesimals forming in the Jupiter-Saturn region. This population of objects would have formed in a faster timescale and in a hotter region of the nebula than their Kuiper belt counterparts, yet still outside the snowline. With the possible exception of  $\sim 100$  km Phoebe, which may itself be at least partially differentiated (Johnson et al. 2009), and whose composition appears to match that of other outer solar nebula objects (Johnson and Lunine 2005), there are no known examples of this population.

Our simplified treatment follows along the same lines as that of other works only applied to our region of interest. We leave a more accurate study for later work (in collaboration with M. Podolak). We solve the energy balance equation for a body of size  $r$  up to the melting temperature  $T_m$  in a time  $t_m$  (e.g., Jewitt et al. 2007)

$$c_p(T) \frac{dT}{dt} = x_r \sum_j \tau_j \gamma_{0,j} H_j - \frac{3k(T)T}{r^2 \rho_p}, \quad (8)$$

where  $\rho_p$  is the mean density,  $x_r$  is the mass fraction of rock,  $\tau_j$ ,  $\gamma_{0,j}$ , and  $H_j$  are the half-life, initial abundance and decay energy per unit mass of radioisotope  $j$ , and  $T$  is the mean

temperature. The conductivity  $k(T)$  and specific heat  $c_p(T)$  are given in terms of their respective values for rock ( $r$ ) and ice ( $i$ ) by (e.g., Multhaup and Spohn 2007)

$$\begin{aligned} k(T) &= k_r f_r + (1 - f_r) k_i(T) \\ c_p(T) &= c_r x_r + (1 - x_r) c_i(T) \end{aligned} \quad (9)$$

where  $f_r$  is the rock volume fraction. In addition, the conductivity and density are adjusted by factors of  $1 - \phi^{2/3}$  and  $1 - \phi$ , respectively, to account for porosity  $\phi$  (Smoluchowski 1981). Equation 8 yields the temperature of the planetesimal subject to radionuclide heating and conductive cooling. The relevant parameters for these calculations are given in Table 2.

A variety of outcomes are possible depending on poorly constrained model parameters, but melting is likely to take place if the object incorporates a significant amount of  $^{26}\text{Al}$ . A study by Merk and Prialnik (2006) that includes radioactive heating, accretion, transformation of amorphous to crystalline ice and melting of water ice in the formation of trans-neptunian objects with sizes  $\sim 10$  km finds that the occurrence of liquid water may be common. Since Kuiper belt objects form in longer timescale and accrete in a colder environment, it is not surprising that planetesimals forming early-on in the Jupiter-Saturn region are prone to melting. In Fig. 7 we show the mean temperature as function of time for several values of the delay between CAIs and planetesimal formation (assuming  $^{26}\text{Al}$  is homogeneously distributed out to Saturn). The nebula temperature is 100 K. The values for the physical parameters used in this model are given in Table 1. We start with crystallized ice (and no CO), due to our higher temperature of accretion. We ignore serpentinization reactions, which would lead to further heating. Melting of these objects is difficult to avoid in the Jupiter-Saturn region even with significant delays in the planetesimal formation time. The reason is that the energy supply of  $^{26}\text{Al}$  greatly exceeds the amount of energy required for melting the entire object. For a planetesimal of size  $\sim 10$  km, conduction cannot remove this energy in time, leading to at least partial differentiation. This also fits with more detailed studies of hydrological activity of small icy planetesimals in the asteroid belt (Young 2001), where the background temperature is higher. The disruption of partially differentiated planetesimals would then lead to a population of icy/rocky fragments available to ablate through the extended Kronian gas disk.

Above we neglect heat transport by water vapor flow through a porous medium driven by internal sublimation (Prialnik and Podolak 1995). Yet, the presence of liquid water is not required for partial differentiation to take place. Enhanced conductivity by water vapor flow through porous media may discourage melting, but would still result in a layered internal state as the core would become water-depleted (Prialnik et al. 2008). To check this we add a cooling term due to the rate of vapor sublimation given by (e.g., Prialnik and Podolak 1995)

$$Q_v = S_\phi H_v (\mathcal{P}(\mathcal{T}) - P_v) \left( \frac{\mu_{\text{ice}}}{2\pi R_g T} \right)^{1/2} \quad (10)$$

where  $S_\phi = -(3/r_0)\phi \ln \phi$  is the surface to volume ratio (Koponen et al. 1997),  $r_0$  is the grain size,  $H_v$  is the latent heat of vaporization,  $\mathcal{P}(\mathcal{T})$  is the saturated vapor pressure,

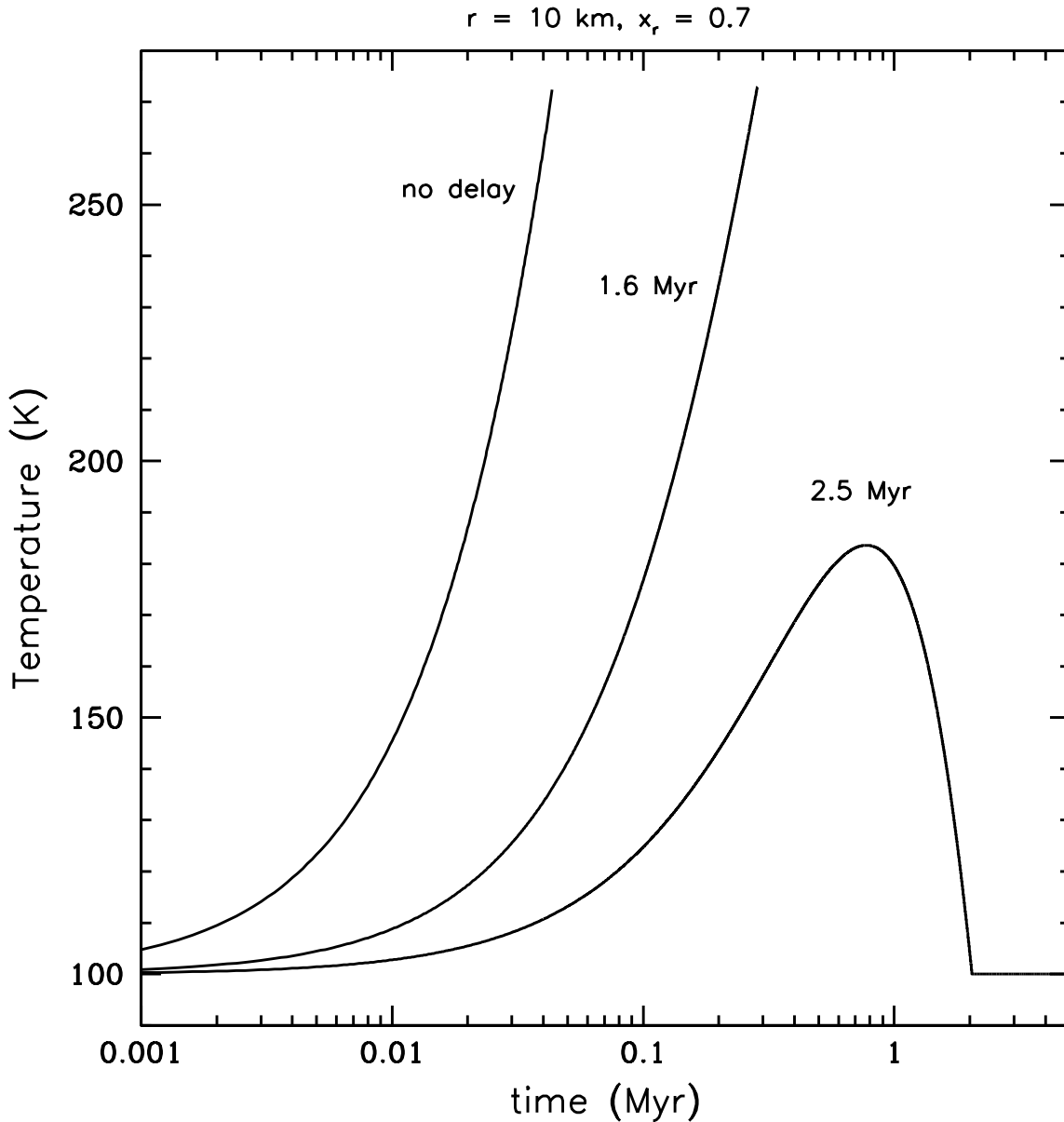


Figure 7: Mean planetesimal temperature as a function of time. The curves correspond to different delay times between CAIs and the formation time of the primordial 10 km planetesimal. The rock fraction is  $x_r = 0.7$  by mass. The porosity is  $\phi = 0.3$ . Since planetesimals in the Jupiter-Saturn region form in the first  $\sim 1$  Myr they are expected to reach melting temperatures.

$P_v$  is the gas pressure,  $\mu_{ice}$  is the molecular mass of ice, and  $R_g$  is the gas constant. The value for the porosity is uncertain and the sublimation rate is model-dependent. We treat it as an adjustable parameter and find that for values relevant to the Jupiter-Saturn region with nebula temperature  $\sim 100$  K and significant quantities of  $^{26}\text{Al}$  one must sublimate a significant fraction of the water-ice of the object in order to keep it from melting. Thus, whether sublimation is sufficiently effective to preclude melting or not, radiogenic heating

is likely to result in separation of rock and water in our regime of interest where nebula temperatures are higher and accretion timescales shorter than in the Kuiper belt, which leads us to expect that the primordial population of planetesimals in the Jupiter-Saturn region is partially differentiated.

Table 2: Thermal evolution parameters

---

Thermal conductivity of ice <sup>a</sup>
$k_i = 4.8812 \times 10^7 / T + 0.4685 \times 10^5$ (g cm s <sup>-3</sup> )
Thermal conductivity of water
$k_w = 0.55 \times 10^5$ (g cm s <sup>-3</sup> )
Thermal conductivity of rock <sup>b</sup>
$k_r = 4.2 \times 10^5$ (g cm s <sup>-3</sup> )
Specific heat of ice <sup>a</sup>
$c_i = 7.037 \times 10^4 T + 1.85 \times 10^6$ (cm <sup>2</sup> K <sup>-1</sup> s <sup>-2</sup> )
Specific heat of water
$c_w = 4.19 \times 10^7$ (cm <sup>2</sup> K <sup>-1</sup> s <sup>-2</sup> )
Specific heat of rock <sup>b</sup>
$c_r = 1.2 \times 10^7$ (cm <sup>2</sup> K <sup>-1</sup> s <sup>-2</sup> )
Half life of <sup>26</sup> Al = $7.2 \times 10^5$ yrs
Initial abundance of <sup>26</sup> Al = $7.0 \times 10^{-7}$ from $\frac{^{26}\text{Al}}{^{27}\text{Al}} = 5 \times 10^{-5}$
Heat production rate <sup>c</sup> of <sup>26</sup> Al = $1.16 \times 10^{17}$ (erg g <sup>-1</sup> )

---

<sup>a</sup>Hobbs (1974); <sup>b</sup>Ellsworth and Schubert (1983); <sup>c</sup>Castillo-Rogez et al. (2009)

## 5 Conclusions

There are two self-consistent models of satellite formation (MEa,b; Estrada and Mosqueira 2006; see Estrada *et al.* 2009 for a review). Both of these models treat planetesimal dynamics explicitly and derive the solids leading to the formation of the regular satellites from the “shower” of planetesimal fragments following the formation of the giant planets. However, only one of the two accretes satellites in the presence of a relatively massive (SEMM) gas component (MEa,b; see Mosqueira *et al.* 2009 for a review) able to ablate and capture a significant fraction of the planetesimal rubble crossing the circumplanetary disk. Simply put, there are two basic options available to modelers: first, guided by the distribution of satellite mass for Jupiter and Saturn (especially but not exclusively the large separation between Titan and Iapetus), one can infer a *gaseous* subnebula with a relatively dense inner region and a long tail out to the location of the irregular satellites; second, assuming instead that the gas component is dissipated by an *unknown* mechanism in a short timescale, one can consider a *gas-poor* satellite formation model.

Here we show that it is possible to understand the mass budgets and compositions of



the regular satellites of the giant planets in terms of a two-component gaseous model<sup>5</sup>. In particular, the result that (even allowing for porosity) Iapetus is water-ice rich compared to solar mixtures provides strong support for the presence of a two-component (SEMM) gas disk at the time of satellite formation. Indeed, a lower surface density outer disk is *required* to simultaneously satisfy the constraints imposed by Iapetus' small mass and ice-rich composition (compared to Callisto, Ganymede and Titan). Thus, Iapetus' distance from the primary sets it apart from all other regular satellites. But we stress that our framework applies in general to the formation of regular satellites around gaseous giants. In fact, our results also account for the water-ice enrichment of Callisto compared to Ganymede as observed.

For our model to apply, the first generation of planetesimals in the Jupiter-Saturn region must be at least partially differentiated. We conduct a preliminary investigation of the thermal evolution of planetesimals, and find that 10 km bodies in Jupiter-Saturn region are more likely to melt and differentiate than similar composition and size objects located in the Kuiper belt region because of the shorter accretion times and hotter nebula environment closer to the Sun. Since we argue that the first generation of planetesimals in the Jupiter-Saturn region form quickly and incorporate significant quantities of <sup>26</sup>Al, these objects are at least partially differentiated. As a result, the collisional cascade following giant planet formation leads to the production of a non-homogeneous population of planetesimal fragments available to ablate through the circumplanetary disks of the giant planets, resulting in water-ice enrichment in the outer disk. Given the small degree of radial mixing expected in the quiescent-disk SEMM satellite formation model (MEa,b), a radial compositional gradient can be preserved in the bulk properties of the regular satellites as observed.

We do not include the abundances of other volatile species, as we do not have good constraints for their contribution to the bulk compositions of either Kuiper belt objects or regular satellites. Also, we do not consider a phase of condensed, refractory carbon (in contrast to CH<sub>4</sub>, which is trapped in water-ice). Solid carbon affects the condensate density and reduces the amount of CO available to sequester oxygen (Johnson and Lunine 2005; Wong et al. 2008). However, there is presently no evidence that such a phase plays a significant role in the bulk compositions of the regular satellites, and no reason for including it in Iapetus but not doing so in other regular satellites, Phoebe, or Kuiper belt objects. Although a number of the parameters employed here are at present uncertain, our work ties regular satellite formation to the outer solar nebula, so that constraints from observational studies of the compositions of the giant planets, or comet populations, and further theoretical work of the requirements for giant planet core formation, or Kuiper belt constraints, can be used in connection with the regular satellites as well. In fact, this is the first study to establish a direct link between solar nebula planetesimals and the bulk properties of regular satellites, thus opening up an entirely new research direction. A number of effects have been left for further work, notably: collisional damping in the planetesimal dynamics following giant planet formation, and the effect of multiple disk crossings for those objects that are

---

<sup>5</sup>A two component model has the added benefit of providing a natural explanation for the Callisto-Ganymede dichotomy without resorting to fine-tuning model parameters (see Estrada et al. 2009 and Mosqueira et al. 2009). This also fits with the observation that the composition of Callisto is icier than that of Ganymede.

not captured during the first pass. Also, our results assume that the size distribution and size cut-offs, and velocity at infinity of rocky and icy fragments are the same.

However, we have tested parameter sensitivities and find that the result that the outer disk of Saturn is ice-rich compared to its inner disk, and also compared to the outer solar nebula, is robust, provided that primordial planetesimals are at least partially differentiated. The reason is that delivery of solids in the outer disk is dominated by melting and vaporization of water-ice at temperatures of hundreds of degrees Kelvin. This result is a consequence of the lower gas surface density and lower planetesimal velocities in the outer disk. Consequently, icy fragments of size  $\gtrsim 1$  m are delivered by ablation (and some capture), whereas delivery of rocky fragments of similar size is highly inefficient. This is mainly because the temperature of objects crossing the outer disk is not high enough for rock to melt or vaporize. Additionally, overall a higher proportion of the rock content is delivered by capture, which drops off as the surface density gets lower. This is because for less pronounced ablation the cross section of the traversing planetesimal and gas drag force are larger, resulting in a higher proportion of mass captured compared to ablated. Also, rocky objects are more difficult to capture for a given object size due to their greater density but this may be compensated by the availability of somewhat smaller rocky fragments.

Still, much work remains to be done to pin down the degree of enrichment quantitatively; in particular, while second pass-capture of rocky fragments does not erase a subnebula compositional gradient signature, it can deliver rock to the disk via capture and should be explored. Also, while collisional damping of planetesimal eccentricities does not prevent delivery of collisional rubble to the circumplanetary disk during close encounters with the giant planet, the amount of mass delivered is likely to be affected, as it depends on the mass spectrum. Moreover, other delivery mechanisms, such as collisional capture and three-body effects, may also contribute to the mass budget of the regular satellites but have not been included in our analysis. Finally, we assume a starting condition of a gas disk without solid content. Yet planetesimals dissolve in the gas giant envelope, thus enhancing the planet's metallicity (Pollack et al. 1986) and possibly the gas disk as well. Most of this mass delivery takes place before the mass of the gaseous envelope grows larger than that of the core. This is then followed by a *dilution* during runaway gas accretion (Pollack et al. 1996). It is unclear whether this source of solids will contribute significantly to the regular satellites, especially to those located far from the planet. We expect that the outer disk forms *after* envelope collapse, as the giant planets open a gap in the nebula, and that this gas is relatively free of solids (see Estrada et al. 2009 for further discussion). Moreover, dust settling in the envelope of the giant planet may also limit the solid content that is left behind in the subnebula far from the planet. Ice/rock fractionation is also possible. We leave this issue for further work.

*Acknowledgements.* We would like to thank Jay Melosh and Uma Gorti for useful discussions. I. Mosqueira's research is supported by NASA PG&G, and OPR grants. P. Estrada contribution is supported by a NASA OSS grant.

## References

- Anderson, J. D., Johnson, T. V., Schubert, G., Asmar, S, Jacobson, R. A., Johnston, D., Lau, E. L., Lewis, G., Moore, W. B., Taylor, A., Thomas, P. C., and G. Weinwurm 2005. Amalthea's density is less than that of water. *Science*, **308**, 1291-1293.
- Atreya, S. K., Wong, M. H., Owen, T. C., Mahaffy, P. R., Niemann, H. B., de Pater, I., Drossart, P., Encrenaz, T., 1999. A comparison of the atmospheres of Jupiter and Saturn: deep atmospheric composition, cloud structure, vertical mixing, and origin. *Plan. and Space Sci.* **47**, 1243-1262.
- Ayliffe B., and Bate M. R., 2009. Circumplanetary disc properties obtained from radiation hydrodynamical simulations of gas accretion by protoplanets. *M.N.R.A.S* **397**, 657-665.
- Bai, X., Goodman, J., 2009. Heat and Dust in Active Layers of Protostellar Disks. *Astrophys. J.* **701**, 737-755.
- Baker, J., Bizzarro, M., Wittig, N., Connelly, J., Haack, H., 2005. Early planetesimal melting from an age of 4.5662Gyr for differentiated meteorites. *Nature* **436**, 1127-1131.
- Bate, M. R., Lubow, S. H., Ogilvie, G. I., and K. A. Miller 2003. Three-dimensional calculations of high- and low-mass planets embedded in protoplanetary discs. *M.N.R.A.S.*, **341**, 213-229.
- Beckwith, S. V. W., Henning, T., and Nakagawa, Y., 2000. Dust properties and assembly of large particles in protoplanetary disks. In *Protostars and Planets IV*. Eds., V. Mannings, A. P. Boss, and S. S. Russell, University of Arizona Press, 533-558.
- Bell, K. R., Cassen, P. M., Wasson, J. T., Woolum, D. S., 2000. The FU Orionis phenomenon and solar nebula material. In *Protostars and Planets IV*. Eds., V. Mannings, A. P. Boss, and S. S. Russell, University of Arizona Press, 897-926.
- Benz, W., and E. Asphaug 1999. Catastrophic disruptions revisited. *Icarus*, **142**, 5-20.
- Birnstiel, T., Dullemond, C. P., Brauer, F., 2009. Dust retention in protoplanetary disks. *Astron. & Astrophys.* In press.
- Bodenheimer, P., and J. B. Pollack 1986. Calculations of the accretion and evolution of the giant planets: The effects of solid cores. *Icarus* **67**, 391-408.
- Bottke, W. F., Durda, D. D., Nesvorny, D., Jedicke, R., Morbidelli, A., Vokrouhlicky, D., Levison, H. F., 2005. Linking the collisional history of the main asteroid belt to its dynamical excitation and depletion. *Icarus* **179**, 63-94.
- Brauer, F., Henning, Th., Dullemond, C. P., 2008. Planetesimal formation near the snow line in MRI-driven turbulent protoplanetary disks. *Astron. & Astrophys.* **487**, L1-L4
- Bronshten, V. A., 1983. Ablation of meteoroids. *Meteo. Iss.* **8**, 38-50. In Russian.
- Brown, M. E., Schaller, E. L., 2007. The Mass of Dwarf Planet Eris. *Science* **316**, 1585.
- Buie, M. W., Grundy, W. M., Young, E. F., Young, L. A., Stern, S. A., 2006. Orbits and Photometry of Pluto's Satellites: Charon, S/2005 P1, and S/2005 P2. *Astron. J.* **132**, 290-298.

- Buratti, B. J., Hicks, M. D., Lawrence, K. J., 2009. Movement of Low-albedo Dust from Small Irregular Satellites to the Main Satellites of the Outer Planets. *BAAS* **41**.
- Canup, R. M., W. R. Ward 2002. Formation of the Galilean Satellites: Conditions of Accretion. *Astron. J.* **124**, 3404-3423.
- Cassen, P., and Pettibone, D. 1976. Steady accretion of a rotating fluid. *Astrophys. J.* **208**, 500-511.
- Castillo-Rogez, J. C., Matson, D. L., Sotin, C., Johnson, T. V., Lunine, J. I., Thomas, P. C., 2007. Iapetus' geophysics: Rotation rate, shape, and equatorial ridge. *Icarus* **190**, 179-202.
- Castillo-Rogez, J., Johnson, T. V., Lee, M. H., Turner, N. J., Matson, D. L., Lunine, J., 2009.  $^{26}\text{Al}$  decay: Heat production and a revised age for Iapetus. *Icarus*. In press.
- Chabot, N. L., Haack, H., 2006. Evolution of Asteroidal Cores. In *Meteorites and the Early Solar System II*. Eds., D. S. Lauretta, and H. Y. McSween Jr., University of Arizona Press, 747-771.
- Charnoz, S., and A. Morbidelli 2003. Coupling dynamical and collisional evolution of small bodies: an application to the early ejection of planetesimals from the Jupiter-Saturn region. *Icarus*, **166**, 141-156.
- Charnoz, S., Morbidelli, A., 2007. Coupling dynamical and collisional evolution of small bodies. II. Forming the Kuiper belt, the Scattered Disk and the Oort Cloud. *Icarus***188**, 468-480.
- Charnoz S., Morbidelli, A., Dones, L., and Salmon, J. 2009. Did Saturn's rings form during the Late Heavy Bombardment? *Icarus* **199**, 413-428.
- Currie, T., Lada, C. J., Plavchan, P., Robitaille, T. P., Irwin, J., Kenyon, S. J., 2009. The Last Gasp of Gas Giant Planet Formation: A Spitzer Study of the 5 Myr Old Cluster NGC 2362. *Astrophys. J.* **698**, 1-27.
- Cuzzi, J.N.; Estrada, P.R., 1998. Compositional evolution of Saturn's rings due to meteoroid bombardment. *Icarus* **132**, 1-35.
- Cuzzi, J. N., Hogan, R. C., Shariff, K., 2008. Toward Planetesimals: Dense Chondrule Clumps in the Protoplanetary Nebula. *Astrophys. J.* **687**, 1432-1447.
- Cuzzi, J. N., and Weidenschilling S., 2006. Particle gas dynamics and primary accretion. In *Meteors and the Early Solar System II*. Eds., D. Lauretta, L. A. Leshin, and H. McSween, University of Arizona Press, 353-381.
- Chyba, C. F., 1993. Explosions of small Spacewatch objects in the Earth's atmosphere. *Nature* **363**, 701-703.
- Davis, D. R., Farinella, P., 1997. Collisional Evolution of Edgeworth-Kuiper Belt Objects. *Icarus* **125**, 50-60.
- Dodson-Robinson, S. E., Bodenheimer, P., Laughlin, G., Willacy, K., Turner, N. J., Beichman, C. A., 2008. Saturn Forms by Core Accretion in 3.4 Myr. *Astrophys. J.* **688**, L99-L102

- Dohnanyi, J. W., 1969. Collisional model of asteroids and their debris. *J. Geophys. Res.* **74**, 2531-2554.
- Dominik, C., Blum, J., Cuzzi, J. N., Wurm, G., 2007. Growth of Dust as the Initial Step Toward Planet Formation. In *Protostars and Planets V*. Eds., B. Reipurth, D. Jewitt, and K. Keil, University of Arizona Press, Tucson, 783-800.
- Dominik, C., Dullemond, C. P., 2008. Coagulation of small grains in disks: the influence of residual infall and initial small-grain content. *Astron. & Astrophys.* **491**, 663-670.
- Dullemond, C. P., Dominik, C., 2005. Dust coagulation in protoplanetary disks: A rapid depletion of small grains *Astron. & Astrophys.* **434**, 917-986.
- Durham, W. B., McKinnon, W. B.; Stern, L. A., 2005. Cold compaction of water ice. *Geophys. Res. Lett.* **32** L18202.
- Ellsworth, K., and Schubert, G., 1983. Saturn's icy satellites: thermal and structural models. *Icarus* **54**, 490-510.
- Estrada, P. R., and I. Mosqueira 2006. A gas-poor planetesimal capture model for the formation of giant planet satellite systems. *Icarus* **181**, 486-509.
- Estrada, P. R., I. Mosqueira, J. J. Lissauer, G. D'Angelo, D. P. Cruikshank 2009. Formation of Jupiter and Conditions for Accretion of the Galilean Satellites. To appear in the Europa Book, Eds. W. McKinnon, R. Pappalardo, and K. Khurana. University of Arizona Press.
- Ghosh, A., Weidenschilling, S. J., McSween, H. Y., Jr., Rubin, A., 2006. Asteroidal Heating and Thermal Stratification of the Asteroidal Belt. In *Meteorites and the Early Solar System II*. Eds., D. S. Lauretta and H. Y. McSween Jr., University of Arizona Press, 555-566.
- Hayashi, C., 1981. Structure of the solar nebula, growth and decay of magnetic fields, and effects of magnetic and turbulent viscosities on the nebula. *Prog. Theor. Phys. Suppl.*, **70**, 35-53.
- Hobbs, P. V., 1974 *Ice Physics*, Oxford University Press, London. pp. 347-363.
- Housen, K. R., Schmidt, R. M., Holsapple, K. A., 1991. Laboratory simulations of large-scale fragmentation events. *Icarus* **94**, 180-190.
- Hubickyj, O., Bodenheimer, P., and J. J. Lissauer 2005. Accretion of the gaseous envelope of Jupiter around a 5 – 10 Earth-mass core. *Icarus* **179**, 415-431.
- Jacobson, R. A., Antreasian, P. G., Bordi, J. J., Criddle, K. E., Ionasescu, R., Jones, J. B., Mackenzie, R. A., Meek, M. C., Parcher, D., Pelletier, F. J., Owen, W. M., Roth, Jr., D. C., Roundhill, I. M., and J. R. Stauch 2006. The gravity field of the saturnian system from satellite observations and spacecraft tracking data. *Astron. J.*, **132**, 2520-2526.
- Jewitt, D., Chizmadia, L., Grimm, R., Prialnik, D., 2007. Water in the Small Bodies of the Solar System. In *Protostars and Planets V*. Eds., B. Reipurth, D. Jewitt, and K. Keil, University of Arizona Press, 863-878.
- Johansen, A., Oishi, J. S., Low, M. M., Klahr, H., Henning, T., Youdin, A., 2007. Rapid planetesimal formation in turbulent circumstellar disks *Nature* **448**, 1022-1025.

- Johnson, T. V., and J. I. Lunine 2005. Density-derived constraints on the origin of Saturn's moon Phoebe. *Nature*, **435**, 67-71.
- Johnson T.V., Castillo-Rogez J. C., Matson D. L., Thomas P. C., 2009. Phoebe's shape: possible constraints on internal structure and origin. 40th Lunar and Planetary Science Conference.
- Kenyon, S. J., and Luu, J. X. 1999. Accretion in the early Kuiper Belt. II. Fragmentation. *Astrophys. J.* **118**, 1101-1119.
- Koponen, A., Kataja, M., Timonen, J., 1997. Permeability and effective porosity of porous media. *Phys. Rev. E* **56**, 3319-3325.
- Kretke, K. A., Lin, D. N. C., 2007. Grain Retention and Formation of Planetesimals near the Snow Line in MRI-driven Turbulent Protoplanetary Disks. *Astrophys. J.* **664**, L55-L58.
- Lin, D. N. C., and J. Papaloizou 1993. On the tidal interaction between protostellar disks and companions. In *Protostars and Planets III* (E. H. Levy and J. I. Lunine, Eds.) pp. 749-836, Univ. of Arizona, Tucson.
- Lunine. J. I., and Stevenson, D. J. 1982. Formation of the Galilean satellites in a gaseous nebula. *Icarus* **52**, 14-39.
- Lyra, W., Johansen, A., Zsom, A., Klahr, H., Piskunov, N., 2009. Planet formation bursts at the borders of the dead zone in 2D numerical simulations of circumstellar disks. *Astron. & Astrophys.* **497**, 869-888.
- McKinnon, W. B., Simonelli, D. P., and G. Schubert 1997. Composition, internal structure, and thermal evolution of Pluto and Charon. In: Stern, A., Tholen, D. J. (Eds.), Pluto and Charon. Univ. of Arizona Press, Tucson, p.295.
- Melosh, H. J., Nimmo, F., 2009. An Intrusive Dike Origin for Iapetus' Enigmatic Ridge? 40th Lunar and Planetary Science Conference.
- Merk R., Prialnik D., 2006. Combined modeling of thermal evolution and accretion of trans-neptunian objects – Occurrence of high temperatures and liquid water. *Icarus* **183**, 283-295.
- Morbidelli, A., Bottke, W., Nesvorny, D., Levison, H. F., 2009. Asteroids Were Born Big. *Icarus*. In press.
- Morbidelli, A., Levison, H. F., Gomes, R., 2008. The Dynamical Structure of the Kuiper Belt and Its Primordial Origin. In *The Solar System Beyond Neptune*. Eds., M. A. Barucci, H. Boehnhardt, D. P. Cruikshank, and A. Morbidelli, University of Arizona Press, 275-292.
- Morfill G.E., Fechtig H., Grn E., and Goertz C.K., 1983. Some consequences of meteoroid impacts on Saturns rings. *Icarus* **55**, 439-447.
- Moses, J., 1992. Meteoroid ablation in Neptune's atmosphere. *Icarus* **99**, 368-383.
- Mosqueira, I., 2004. On Planet-Satellite Formation. Presented at the KITP Program: Planet Formation: Terrestrial and Extra Solar, Kavli Institute for Theoretical Physics, University of California, Santa Barbara.

- Mosqueira, I. and Estrada, P. R. 2003a. Formation of large regular satellites of giant planets in an extended gaseous nebula. I. Subnebula model and accretion of satellites. *Icarus* **163**, 198-231.
- Mosqueira, I. and Estrada, P. R. 2003b. Formation of large regular satellites of giant planets in an extended gaseous nebula. II. Satellite migration and survival. *Icarus* **163**, 232-255.
- Mosqueira, I., Estrada, P. R., 2005. On the origin of the Saturnian satellite system: Did Iapetus form in-situ? 36th LPSC meeting, Houston, TX, no. 1951.
- Mosqueira, I., Estrada, P. R., and Turrini, D., 2009. Planetesimals and satellitesimals: the accretion of the regular satellites. 2nd ISSI-Europlanet Workshop Book. Submitted.
- Multhaup, K., and T. Spohn 2007. Stagnant lid convection in the mid-sized icy satellites of Saturn. *Icarus* **186**, 420-435.
- Niemann, H. B., Atreya, S. K., Bauer, S. J., Carignan, G. R., Demick, J. E., Frost, R. L., Gautier, D., Haberman, J. A., Harpold, D. N., Hunten, D. M., Israel, G., Lunine, J. I., Kasprzak, W. T., Owen, T. C., Paulkovich, M., Raulin, F., Raaen, E., Way, S. H., 2005. The abundances of constituents of Titan's atmosphere from the GCMS instrument on the Huygens probe. *Nature* **438**, 779-784.
- Owen, T., Encrenaz, T., 2003. Element Abundances and Isotope Ratios in the Giant Planets and Titan. *Space Sci. Rev.* **106**, 121-138.
- Person, M. J., Elliot, J. L., Gulbis, A. A. S., Pasachoff, J. M., Babcock, B. A., Souza, S. P., Gangestad, J., 2006. Charon's Radius and Density from the Combined Data Sets of the 2005 July 11 Occultation. *Astron. J.* **132**, 1575-1580.
- Podolak, M., Pollack, J. B., Reynolds, R. T., 1988. Interactions of planetesimals with protoplanetary atmospheres. *Icarus* **73**, 163-179.
- Pollack, J. B., A. S. Grossman, R. Moore, and H. C. Graboske, Jr. 1976. The formation of Saturn's satellites and rings as influenced by Saturn's contraction history. *Icarus* **29**, 35-48.
- Pollack, J. B., O. Hubickyj, P. Bodenheimer, J. J. Lissauer, M. Podolak, and Y. Greenzweig 1996. Formation of the giant planets by concurrent accretion of solids and gas. *Icarus* **124**, 62-85.
- Pollack, J. B., Podolak, M., Bodenheimer, P., and B. Christofferson 1986. Planetesimal dissolution in the envelopes of the forming, giant planets. *Icarus*, **67**, 409-443.
- Pollack J. B., Reynolds R. T., 1974. Implications of Jupiter's early contraction history for the composition of the Galilean satellites. *Icarus* **21**, 248-253.
- Prialnik D., Podolak M., 1995. Radioactive heating of porous comet nuclei. *Icarus* **117**, 420-430.
- Prialnik D., Sarid G., Rosenberg E. D., Merk R., 2008. Thermal and chemical evolution of comet nuclei and Kuiper belt objects. *Space Sci. Rev.* **138**, 147-164.
- Prinn R. G., Fegley B., 1981. Kinetic inhibition of CO and N<sub>2</sub> reduction in circumplanetary nebulae: implications for satellite composition. *Astrophys. J.* **249**, 308-317.

- Rafikov, R. R. 2002. Planet migration and gap formation by tidally induced shocks. *Astrophys. J.* **572**, 566-579.
- Ruskol, Y. L. 1975. Origin of the Moon. Origin of the moon NASA Transl. into english of the book "Proiskhozhdeniye Luny" Moscow, Nauka Press, 1975 1-188.
- Ryan, E. V., Davis, D. R., Giblin, I., 1999. A Laboratory Impact Study of Simulated Edgeworth-Kuiper Belt Objects. *Icarus* **142**, 56-62.
- Scott, E. R. D., Krot, A. N., 2005. Chondritic Meteorites and the High-Temperature Nebular Origins of Their Components. In *Chondrites and the Protoplanetary Disk.*, ASP Conference Series, **341**. Eds., A. N. Krot, E. R. D. Scott, and B. Reipurth. Astronomical Society of the Pacific, p.15.
- Smoluchowski, R. 1981. Heat content and evolution of cometary nuclei. *Icarus* **47**, 312-319.
- Sohl, F., Spohn, T., Breuer, D., Nagel, K., 2002. Implications from Galileo Observations on the Interior Structure and Chemistry of the Galilean Satellites. *Icarus* **157**, 104-119.
- Stern, S. A., and P. R. Weissman 2001. Rapid collisional evolution of comets during the formation of the Oort cloud. *Nature*, **409**, 589-591.
- Stevenson, D. J., A. W. Harris, and J. I. Lunine 1986. Origins of satellites. In *Satellites* (J. A. Burns and M. S. Matthews, Eds.) Univ. of Arizona Press, Tucson.
- Svetsov, V. V., Nemtchinov, I. V., and Teterov, A. V., 1995. Disintegration of large meteoroids in Earth's atmosphere: Theoretical models. *Icarus* **116**, 131-153.
- Tamayo, D., Burns, J. A., Denk, T., 2009. Dynamical Models for the Origin of Iapetus' Dark Material. *BAAS* **41**.
- Tanaka, H., T. Takeuchi, W. R. Ward 2002. Three-dimensional interaction between a planet and an isothermal gaseous disk. I. Corotation and Lindblad torques and planet migration. *Astrophys. J.* **565**, 1257-1274.
- Thomas, P. C., Veverka, J., Helfenstein, P., Porco, C., Burns, J., Denk, T., Turtle, E., Jacobson, R. A., 2006. Shapes of the Saturnian Icy Satellites 37th Annual Lunar and Planetary Science Conference.
- Tremaine, S., Touma, J., Namouni, F., 2009. Satellite Dynamics on the Laplace Surface. *Astron. J.* **137**, 3706-3717.
- Tsiganis K., Gomes R., Morbidelli A., Levison H. F., 2005. Origin of the orbital architecture of the giant planets of the Solar System. *Nature* **435**, 459-461.
- Turner, N. J., Sano, T., Dziourkevitch, N., 2007. Turbulent Mixing and the Dead Zone in Protostellar Disks. *Astrophys. J.* **659**, 729-737.
- Ward, W. R., 1981. Orbital inclination of Iapetus and the rotation of the Laplacian plane. *Icarus* **46**, 97-107.
- Weidenschilling, S. 1997. The origin of comets in the solar nebula: A unified model. *Icarus*, **127**, 290-306.
- Weidenschilling, S. J., 2000. Formation of Planetesimals and Accretion of the Terrestrial Planets. *Space Sci. Rev.* **92**, 295-310.



- Weidenschilling, S. J., 2009. How Big Were the First Planetesimals? Does Size Matter? 40th Lunar and Planetary Science Conference.
- Wetherill, G. W., and G. R. Stewart 1993. Formation of planetary embryos - Effects of fragmentation, low relative velocity, and independent variation of eccentricity and inclination. *Icarus*, **106**, 190.
- Youdin, A. N., and F. H. Shu 2002. Planetesimal formation by gravitational instability. *Astrophys. J.* **580**, 494-505.
- Young, E. D., 2001. The hydrology of carbonaceous chondrite parent bodies and the evolution of planet progenitors. *Phil. Trans. R. Soc. Lond.* **359**, 2095-2110.
- Wong, M. H., Lunine, J. I., Atreya, S. K., Johnson, T., Mahaffy, P. R., Owen, T. C., Encrenaz, T., 2008. Oxygen and other volatiles in the giant planets and their satellites. *Rev. Mineralogy and Geochem.* **68**, 219-246.
- Zahnle, K. J., 1992. Airburst origin of dark shadows on Venus. *J. Geophys. Res.* **97**, 243-255.
- Zahnle, K., Mac Low, M., 1994. The collision of Jupiter and Comet Shoemaker-Levy 9. *Icarus* **108**, 1-17.